Original Article

MITOCHONDRIAL TRANSFER FROM ADIPOSE-DERIVED STEM CELLS IMPROVES THE CHONDROGENIC PHENOTYPE IN SENESCENT CHONDROCYTES BY AMELIORATING MITOCHONDRIAL DYSFUNCTION

Chewei Wu[1,2,3,§], Yaohui Huang[4,§], Peilin Shao[5], Linghua Chang[1,2], Chengchang Lu[1,2,6,7,8], Chunghwan Chen[1,2,6,7,8,9,10,11], Yinchih Fu[1,2,7,8,12], Meiling Ho[1,2], Jeken Chang[1,2,7], and Shuncheng Wu[1,2,5,*]

[1]Regenerative Medicine and Cell Therapy Research Center, Kaohsiung Medical University, 807378 Kaohsiung, Taiwan
[2]Orthopaedic Research Center, College of Medicine, Kaohsiung Medical University, 807378 Kaohsiung, Taiwan
[3]Department of Food Science, Yuanpei University of Medical Technology, 300102 Hsinchu, Taiwan
[4]Department of General Medicine, Kaohsiung Medical University Chung-Ho Memorial Hospital, Kaohsiung Medical University, 807378 Kaohsiung, Taiwan
[5]Department of Nursing, Asia University, 413305 Taichung, Taiwan
[6]Department of Orthopedics, Kaohsiung Municipal Siaogang Hospital, Kaohsiung Medical University, 812 Kaohsiung, Taiwan
[7]Department of Orthopedics, Kaohsiung Medical University Hospital, Kaohsiung Medical University, 807378 Kaohsiung, Taiwan
[8]Ph.D. Program in Biomedical Engineering, College of Medicine, Kaohsiung Medical University, 807378 Kaohsiung, Taiwan
[9]School of Medicine, College of Medicine, Kaohsiung Medical University, 807378 Kaohsiung, Taiwan
[10]Institute of Medical Science and Technology, National Sun Yat-sen University, 804 Kaohsiung, Taiwan
[11]Graduate Institute of Materials Engineering, College of Engineering, National Pingtung University of Science and Technology, 912301 Pingtung, Taiwan
[12]Department of Orthopedics, Kaohsiung Show-Chwan Memorial Hospital, 821011 Kaohsiung, Taiwan
[§]These authors contributed equally.

Abstract

Background: Obtaining sufficient chondrocytes by monolayer expansion in vitro is used for articular cartilage tissue engineering. However, chondrocytes lose their chondrogenic phenotype after monolayer expansion via mitochondrial dysfunction-induced senescence. Adipose-derived stem cell mitochondrial transfer (ADSC-MT) improves senescent cell function. We hypothesise that ADSC-MT improves the chondrogenic phenotype of senescent chondrocytes. **Methods:** After monolayer expansion in vitro, chondrocytes were subjected to ADSC-MT. Cell senescence was evaluated via analysis of p16 and p21 expression and senescence-associated β-galactosidase (SA-β-gal) staining. The chondrogenic phenotype was evaluated by measuring collagen type II (Col-II) and collagen type I (Col-I) levels. Oxidative stress was assessed by determining the mitochondrial superoxide and 8-hydroxydeoxyguanosine (8-OHdG) levels. Mitochondrial dysfunction was assessed by determining the mitochondrial membrane potential (MMP) and PGC-1α levels. Finally, SOD-2, SIRT-1, SIRT-3, TFAM, MFN-1, MFN-2, OPA-1, PINK-1 and Parkin levels were used to assess mitochondrial quality control (MQC). **Results:** ADSC-MT-recipient chondrocytes exhibited alleviated senescence with decreased p16 and p21 expression and SA-β-gal staining. The increased Col-II and decreased Col-I expression indicated that the chondrogenic phenotype of the chondrocytes was restored. Decreased mitochondrial superoxide and 8-OHdG levels indicated alleviated oxidative stress. The increased MMP indicated alleviation of mitochondrial dysfunction. For MQC, SOD-2, PGC-1α, TFAM, SIRT-1, and SIRT-3 were upregulated, indicating that antioxidant defences and mitochondrial biogenesis in MQC were increased in ADSC-MT–recipient chondrocytes. PINK-1 and Parkin were downregulated, suggesting that damaged mitochondria were reduced through mitophagy. In contrast, MFN-1, MFN-2, and OPA-1 were not changed, indicating that mitochondrial dynamics were not affected. **Conclusions:** ADSC-MT improves the chondrogenic phenotype of senescent chondrocytes by ameliorating mitochondrial dysfunction.

Keywords: Articular cartilage tissue engineering, chondrocytes, adipose-derived stem cells (ADSC), mitochondrial transfer (MT), senescence, chondrogenic phenotype, mitochondrial dysfunction.

***Address for correspondence**: Shuncheng Wu, Regenerative Medicine and Cell Therapy Research Center, Kaohsiung Medical University, 807378 Kaohsiung, Taiwan; Orthopaedic Research Center, College of Medicine, Kaohsiung Medical University, 807378 Kaohsiung, Taiwan; Department of Nursing, Asia University, 413305 Taichung, Taiwan. E-mail: r930259@kmu.edu.tw.

Introduction

Articular cartilage is a hypoxic and avascular connective tissue consisting of chondrocytes and hyaline cartilage [1,2]. Articular cartilage defects commonly arise from conditions such as arthritis, accidental trauma, tumours, and degenerative processes [2]. Because articular cartilage is avascular tissue with dense extracellular matrices, the healing potential of articular cartilage defects is limited, and untreated defects often progress to osteoarthritis (OA) [1,2]. Articular cartilage defects are leading causes of OA development [3,4]. OA is a common, debilitating, degenerative disease that affects over 240 million people worldwide [5–7]. In recent decades, extensive efforts have been dedicated to regenerating functional hyaline cartilage within articular cartilage defects [8,9]. Chondrocytes are the sole cell type in articular cartilage, and their function is essential for the repair of articular cartilage defects. Chondrocyte-based articular cartilage tissue engineering has been proposed as an effective approach for treating articular cartilage defects [10–12]. Obtaining sufficient chondrocytes by monolayer expansion *in vitro* is a common process in articular cartilage tissue engineering [10–12]. However, chondrocytes lose their chondrogenic phenotype after monolayer expansion *in vitro*, impairing their ability to synthesise hyaline cartilage [4,13]. Chondrocytes show reduced expression of chondrogenic markers, such as collagen type II (Col-II), in hyaline cartilage, whereas cells show increased expression of collagen type I (Col-I), which is characteristic of fibrocartilage [14,15]. Implantation of these chondrocytes results in undesired fibrocartilage formation in the transplantation area [8,16]. Restoring the chondrogenic phenotype of chondrocytes to synthesise hyaline cartilage after monolayer expansion *in vitro* is challenging for chondrocyte-based articular cartilage tissue engineering.

This issue indicates that the loss of the chondrogenic phenotype in chondrocytes is due to the stress triggered by the culture environment *in vitro* [13]. Chondrocytes originally reside in articular cartilage, which is a low-oxygen microenvironment [13]. However, monolayer expansion *in vitro* to obtain sufficient cells occurs under atmospheric oxygen, and chondrocyte senescence occurs [13]. Therefore, senescence is considered the main contributor to the loss of the chondrogenic phenotype in chondrocytes after monolayer expansion *in vitro* [13]. Reducing senescence may be beneficial for restoring the chondrogenic phenotype of chondrocytes. Studies have shown that cell senescence is linked to the accumulation of mitochondrial dysfunction caused by increased oxidative stress [or overproduction of reactive oxygen species (ROS)] [13,17,18]. Mitochondria are the major sites of cellular ROS generation, and intracellular ROS are generated by mitochondria in response to various stimuli or stress, such as apoptotic signalling, integrin signalling, and serum deprivation [19,20]. Although chondrocytes derive most of their energy from glycolysis when they reside in articular cartilage, increased oxidative phosphorylation rates of mitochondria in chondrocytes are found after monolayer expansion *in vitro* [21,22]. Increased oxidative phosphorylation is associated with the generation of ROS, with up to 5% of the oxygen consumed in the electron transport chain diverted into superoxide production, increasing oxidative stress in chondrocytes [21,22]. These findings suggest that mitochondrial dysfunction caused by increased oxidative stress may be critical for senescence in chondrocytes after monolayer expansion *in vitro*.

Intercellular mitochondrial transfer (MT) is a type of cell-to-cell signalling involving the active incorporation of healthy mitochondria into stressed/injured recipient cells [23]. MT by mesenchymal stem cells (MSCs) into recipient cells is involved in MSC-triggered repair of damaged cells [24,25]. Studies have shown that MT by MSCs alleviated tissue or cell damage, such as the repair of heart tissue, ameliorated lung injury and restored neurological damage [26–28]. Adipose-derived stem cells (ADSC) are MSCs that are isolated from adipose tissue and have been studied for many years in the context of articular cartilage tissue engineering [9,29,30]. Importantly, ADSCs are known to provide mitochondria to recipient cells to normalize the function of senescent cells [31,32]. Moreover, ADSC mitochondrial transfer (ADSC-MT) reportedly promotes cell functions that are reduced by ageing or senescence [33,34]. These findings suggest that ADSC-MT may be used to improve the chondrogenic phenotype of chondrocytes through its regulation of cell senescence. In addition, mitochondrial quality control (MQC) is a mechanism that protects mitochondrial health in cells [18,35]. The primary function of MQC is to ensure mitochondrial quality and maintain mitochondrial functions by limiting oxidative damage to mitochondria [18]. MQC, through antioxidant defences, mitochondrial biogenesis, mitochondrial dynamics and mitophagy, ensures the clearance of dysfunctional mitochondria and preserves mitochondrial homeostasis [18,35]. However, whether ADSC-MT alleviates the senescence of chondrocytes via the regulation of MQC to ameliorate mitochondrial dysfunction has rarely been studied.

In this study, we hypothesize that ADSC-MT improves the chondrogenic phenotype of senescent chondrocytes by ameliorating mitochondrial dysfunction. Chondrocytes were cultured and expanded in monolayers *in vitro*, and the monolayer-expanded chondrocytes presented an increased senescent phenotype, oxidative stress and mito-

chondrial dysfunction. To test our hypothesis, we first investigated whether ADSC-MT reduces the senescent phenotype and restores the chondrogenic phenotype of chondrocytes. We also tested the effects of ADSC-MT on oxidative stress and mitochondrial dysfunction in chondrocytes. To determine whether ADSC-MT regulates MQC in chondrocytes, we also analysed changes in antioxidant defences, mitochondrial biogenesis, mitochondrial dynamics and mitophagy in chondrocytes.

Materials and Methods

Culture of Human Chondrocytes and ADSC

Human chondrocytes derived from the human articular cartilage of 3 donors (34, 44 and 50 years old) were purchased from Lonza Bioscience (cat. No. CC-2550, NHAC-kn Articular Chon CGM, cryo amp, USA). The chondrocytes were cultured and expanded in basal medium containing Dulbecco's modified Eagle's medium (DMEM) (cat. No. BW12-604F, Biowhittaker®; Lonza Bioscience, USA) supplemented with 1% nonessential amino acids (NEAA) (cat. No. 11140050, Gibco BRL, USA), 1% penicillin/streptomycin (cat. No. 15140122, Gibco BRL, USA), 1% insulin–transferrin–selenium (ITS) (cat. No. 41400045, Gibco BRL, USA), and 10% foetal bovine serum (FBS) (cat. No. A5670201, Gibco BRL, USA) [36]. The chondrocytes were cultured at 37°C in a humidified 5% CO_2 incubator, and the medium was changed every 2 days until the cells needed to be passaged [36].

ADSCs were isolated and cultured from patient samples according to protocols described in our previous publications [37–40]. Their characterization—including cell morphology, surface markers expression, and multilineage differentiation potential—has also been previously reported [37–40]. Human adipose tissue was obtained from patients with approval from the Ethics Committee (KMUHIRB-E(II)-20220292). After informed consent was obtained, subcutaneous adipose tissue from the gluteal area was collected from the patients during plastic surgery. After 3 g of subcutaneous adipose tissue was isolated from humans, the adipose tissue was minced with scissors. The minced adipose tissue was then digested with 1 mg/mL type IA collagenase (125 U/mg) (cat. No. 17100017, Gibco BRL, USA) at 37°C under 5% CO_2 for 24 h. The digested tissue was centrifuged at 1000 rpm for 5 min, and the pellet was washed twice with phosphate-buffered saline (PBS). The pellet was then resuspended in K-NAC medium for ADSC expansion per the protocol presented in previous reports [37–40]. The K-NAC medium comprised basal keratinocyte serum-free medium (SFM) (cat. No. 17005042, Gibco BRL, USA) supplemented with 25 mg of bovine pituitary extract (cat. No. 17005042, Gibco BRL, USA), 2.5 µg of human recombinant epidermal growth factor (cat. No. 17005042, Gibco BRL, USA), 2 mM N-acetyl-L-cysteine (cat. No. A8199, Sigma-Aldrich, USA), 0.2 mM L-ascorbic acid 2-phosphate sesquimagnesium salt (cat. No. A8960, Sigma-Aldrich, USA), and 5% FBS [37–39]. The cells were cultured and expanded in a humidified atmosphere with 5% CO_2 at 37°C.

Mitochondrial Isolation From ADSC

For ADSC mitochondria isolation, the Thermo Scientific™ Mitochondria Isolation Kit for Cultured Cells (cat. No. 89874, Thermo Scientific, USA) was used. This kit uses a reagent-based method to isolate mitochondria within 40 minutes after cell harvest. Each step is optimized for high mitochondrial yield and minimal structural damage. Following the protocol, an ADSC (2×10^7 cells) suspension was centrifuged in a microcentrifuge tube at 850 × g for 2 min, and the resulting cell pellet was collected. A total of 800 μL of Mitochondria Isolation Reagent A was added to the cell pellet, which was vortexed at medium speed for 5 seconds and then incubated on ice for 2 min. A total of 10 μL of Mitochondria Isolation Reagent B was added to the cell pellet, which was then vortexed at maximum speed for 5 seconds. The tube was incubated on ice for 5 min and vortexed at maximum speed once per min. Then, 800 μL of Mitochondria Isolation Reagent C was added, and the mixture was mixed. The tube was subsequently centrifuged at 700 × g for 10 min at 4°C. The supernatant was transferred to a new tube and centrifuged at 12,000 × g for 15 min at 4°C. The supernatant containing the cytosolic fraction of ADSC was separated from the pellet. The pellet containing isolated ADSC mitochondria was resuspended in 500 μL of Mitochondria Isolation Reagent C and then centrifuged at 12,000 × g for 5 min to collect the ADSC mitochondrial pellet, which was then maintained on ice before transfer to chondrocytes.

ADSC-MT Into Chondrocytes and Study Groups

We used artificial MT for ADSC-MT, which was performed by coculturing ADSC-derived mitochondria and recipient chondrocytes [41,42]. First, chondrocytes at the initial passage (Passage 1: P1) underwent monolayer expansion *in vitro* for an additional 6 passages (Passage 7: P7). For ADSC-MT into chondrocytes, the chondrocytes at P1 or P7 were seeded onto six-well plates at a concentration of 1×10^5 cells/well. Twenty-four hours after cell seeding, the mitochondria (freshly isolated from 2×10^7 ADSC) were suspended in basal medium and cocultured with chondrocytes at 37°C in a humidified 5% CO_2 incubator for 1 h, after which the medium was carefully removed. After ADSC-MT, the recipient chondrocytes were washed with PBS twice, and the cells were subsequently cultured in basal medium at 37°C in a humidified 5% CO_2 incubator. The medium was changed every 2 days. Three groups were examined in this study: (1) the control (C) group, in which chondrocytes at P1 were cultured in basal medium without any ADSC-MT; (2) the monolayer-expanded (ME) group, in which chondrocytes at P7 were cultured in basal medium without ADSC-MT; and (3) the ADSC-MT (AM) group,

in which the chondrocytes at P7 were cultured in basal medium and treated with ADSC-MT. At the indicated time points, chondrocytes from each group were collected for further experimental analysis.

Mitochondrial Uptake by Recipient Chondrocytes After ADSC-MT

The ADSC were cultured with 50 nM MitoSpy™ Red CMXRos (cat. No. 424802, BioLegend, USA) for 30 min in the dark for mitochondrial labelling. MitoSpy-labelled mitochondria were subsequently isolated from ADSC and transferred into chondrocytes per the protocol described earlier. At the indicated time points, the chondrocytes were collected and stained with CellTracker™ Green CMFDA Dye (cat. No. C7025, Invitrogen, USA) for cell labelling. Then, the cells were fixed with 10% formalin for 15 min, and their cell nuclei were stained with 4′,6-diamidino-2-phenylindole (DAPI) (cat. No. D8417, Sigma-Aldrich, USA). The uptake of MitoSpy-labelled mitochondria by chondrocytes was visualized and captured through a LSM700 confocal laser scanning microscope (Zeiss, Weimar, Germany) and an EVOS M7000 imaging system (Thermo Scientific, USA), and subsequently analysed with ImageJ software to quantify the fluorescence area.

Senescence-Associated β-galactosidase (SA-β-gal) Staining

To assess chondrocyte senescence, we used a Senescence β-Galactosidase Staining Kit (cat. No. 9860, Cell Signaling Technology, USA) following the manufacturer's protocol. At the indicated time points, the chondrocytes were washed three times with cold PBS, and then, the cells were fixed for 15 min with 1 mL of fixing buffer at room temperature. For SA-β-gal staining, the cells were mixed with 1 mL of staining solution and incubated overnight at 37°C. Images were obtained via an EVOS M7000 imaging system (Thermo Scientific, USA). Blue-stained cells were considered SA-β-gal positive, and image analysis was performed using ImageJ software to calculate the area of positively stained cells.

Detection and Quantification of Mitochondrial Superoxide

Mitochondrial superoxide was detected by the MitoSOX Red mitochondrial superoxide indicator (cat. No. M36008, Invitrogen, USA). At the indicated time points, the chondrocytes were washed three times with HBSS and incubated with 5 μM MitoSOX for 10 min at 37°C in the dark. After incubation, the cells were washed with HBSS, and the fluorescence intensity was measured with a BioTek Synergy H1 microplate reader at excitation and emission wavelengths of 510 and 580 nm, respectively. Images were obtained via an EVOS M7000 imaging system (Thermo Scientific, USA).

Measurement of 8-hydroxydeoxyguanosine (8-OHdG)

At the indicated points, the chondrocytes were collected. Enzymatic digests of DNA from chondrocytes were analysed by competitive enzyme-linked immunosorbent assays (ELISAs) using a monoclonal antibody against 8-OHdG (8-OHdG Check, cat. No. KOG-200SE, Genox Corp, USA). Fifty microlitres of DNA digest or standard 8-OHdG solution was added to the wells of a 96-well plate precoated with 8-OHdG, 50 μL of the primary antibody (mouse anti-8-OHdG) was added, and the plate was incubated at 37°C for 1 h. After incubation, the wells were washed with 200 μL/well of 0.05% (v/v) Tween 20 in 0.01 M PBS (pH 7.4), 100 μL/well of the secondary antibody was added (peroxidase-conjugated anti-mouse IgG), and the plate was incubated for 1 h at 37°C. Following incubation, peroxidase substrate (*o*-phenylenediamine/hydrogen peroxide/PBS) was added, the mixture was incubated for 30 min with 2 N sulfuric acid, and the absorbance was read at 450 nm.

Mitochondrial Membrane Potential (MMP) Assay

The MMP of chondrocytes was assayed by JC-10 (cat. No. ab112134; Abcam, UK) according to the manufacturer's protocol. Chondrocytes from each group were plated in a 96-well plate (3×10^3 cells/well) and treated with ADSC-MT. Chondrocytes from each group were cultured for an additional 3 days. The cells were washed with PBS and then stained with JC-10. The cells were then incubated at 37°C in a 5% CO_2 incubator for 30 min in the dark. The intensity of fluorescence in JC-10-labelled cells was measured with a Synergy H1 microplate reader at excitation/emission wavelengths of 475/520 nm and 570/590 nm, respectively, for ratio analysis.

Mitochondrial Mass Measurement

Mitochondrial mass in chondrocytes was evaluated using MitoSpy™ Red CMXRos (cat. No. 424802, BioLegend, USA), a mitochondrial localisation probe that labels mitochondria in live cells and serves as an indicator of mitochondrial content. The chondrocytes were cultured with 50 nM MitoSpy™ Red CMXRos for 30 min in the dark for mitochondrial labelling. After staining, cells were washed twice with phosphate-buffered saline (PBS) to remove excess dye. For fixed-cell imaging, cells were subsequently fixed in 4% paraformaldehyde (PFA) for 15 minutes at room temperature and washed with PBS. Fluorescent images were captured using a fluorescence microscope and analysed with ImageJ software to assess fluorescence area.

Mitochondrial Metabolic Analysis

The mitochondrial respiration and metabolic profiles of the chondrocytes were determined using a Seahorse XF96 Extracellular Flux Bioanalyzer (Seahorse Bioscience, USA) to measure the basal and maximal oxygen consumption rates (OCRs) and the extracellular acidifica-

tion rate (ECAR), as suggested by the manufacturer (cat. No. 103015-100; Agilent Technologies, USA). Briefly, chondrocytes were seeded in 96-well microplates containing an XF96 Extracellular Flux analyser with four blank background wells and incubated overnight. After equilibration for 4 h in a non-CO_2 incubator prior to the assay, a 96-well microplate was used for analysis.

For the Mito Stress test, the chondrocytes were analysed under basal conditions after injection of 2 μM oligomycin to inhibit ATP synthase, 1 μM carbonyl cyanide 4-trifluoromethoxy-phenylhydrazone (FCCP) to induce maximal respiration, and 0.5 μM rotenone and antimycin A to inhibit complexes I and III. Basal respiration, maximal respiration, and the spare respiratory capacity were calculated. For the glycolytic rate test, the cells were analysed following injections of 0.5 μM rotenone/antimycin A to inhibit mitochondrial respiration and 50 μM 2-deoxyglucose (2-DG) to inhibit glycolysis. PER, glycoPER, basal glycolysis, the basal proton efflux rate, and compensatory glycolysis were also calculated. All mitochondrial complex inhibitors were purchased from Seahorse Bioscience.

RNA Isolation and Quantitative Real-time Polymerase Chain Reaction (Real-time PCR)

At the indicated points, the chondrocytes were collected. A TOOLSmart RNA Extractor (cat. No. DPT-BD24, Biotools, Taiwan) was used to extract total RNA from these cells. The RNA quality was confirmed by determining the ratio of the absorbance at 260 nm to that at 280 nm by using a Thermo Scientific NanoDrop 1000 spectrophotometer (Thermo Scientific, USA). In accordance with the manufacturer's instructions, a 260/280-nm absorbance ratio between 1.8 and 2.0 indicated the absence of DNA contamination. Subsequently, 0.5–1 μg of total RNA per 20 μL of reaction mixture was reverse-transcribed into cDNA by using the TOOLS Easy Fast RT Kit (cat. No. KRT-BA28, Biotools, Taiwan). Real-time PCR was conducted using TOOLS 2X SYBR qPCR Mix (cat. No. FPT-BB05, Biotools, Taiwan) and a qRT–PCR detection system (Bio-Rad Laboratories, Hercules, CA, USA). The cDNA samples (2-μL samples with a total volume of 25 µL per reaction) were analysed for the genes of interest. Previously published primer sequences were used to detect Col-II, Col-I and glyceraldehyde-3-phosphate-dehydrogenase (GAPDH) [38,40,43–47]. The mRNA levels of these genes were quantified using the following PCR primer pairs: Col-II (forward: CAA CAC TGC CAA CGT CCA GAT; reverse: TCT TGC AGT GGT AGG TGA TGT TCT), Col-I (forward: GGC TCC TGC TCC TCT TAG; reverse: CAG TTC TTG GTC TCG TCA C), and GAPDH (forward: TCT CCT CTG ACT TCA ACA GCG AC; reverse: CCC TGT TGC TGT AGC CAA ATT C). The following cycling conditions were used: incubation at 94°C for 1 min, followed by 35 cycles of denaturation at 94°C for 30 s and annealing and extension at 59°C for 30s. After real-time PCR, a dissociation (melting) curve was generated to determine the specificity of the reaction. The relative mRNA expression level of each target gene was calculated from the threshold cycle (Ct) value of each PCR product and normalised to GAPDH expression by using the comparative Ct method [48]. For each gene of interest, the readings of four wells from each experimental group were collected at every examined time point.

Antibodies

The antibodies used in this study are as follows: CDKN2A/p16INK4a (cat. No. EPR1473, Abcam, UK; 1:1000), p21 (cat. No. ARG57928, Arigo, Taiwan; 1:1000), superoxide dismutase 2 (SOD-2) (cat. No. 24127-1-AP, Proteintech, USA; 1:5000), Sirtuin-3 (SIRT-3) (cat. No. 12186-1-AP, Proteintech, USA; 1:1000), peroxisome proliferator–activated receptor γ coactivator 1α (PGC-1α) (cat. No. A12348, ABclonal, China; 1:1000), Sirtuin-1 (SIRT-1) (cat. No. A11267, ABclonal, China; 1:1000), cytochrome c oxidase IV (COX IV) (cat. No. A11631, ABclonal, China; 1:1000), voltage-dependent anion channel 1 (VDAC-1) (cat. No. GB111939, Wuhan Servicebio Technology, China; 1:1000), PTEN-induced kinase 1 (PINK-1) (cat. No. #6946, Cell Signaling, USA; 1:1000), Parkin RBR E3 ubiquitin protein ligase (Parkin) (cat. No. #4211, Cell Signaling, USA; 1:1000), β-actin (cat. No. A5441, Sigma-Aldrich, USA), α-tubulin (cat. no. ARG65693, Arigo, Taiwan; 1:1000), mitofusin 1 (MFN-1) (cat. No. 13798-1-AP, Proteintech, USA; 1:1000), mitofusin 2 (MFN-2) (cat. No. 12186-1-AP, Proteintech, USA; 1:1000) and optic atrophy 1 (OPA-1) (cat. No. 27733-1-AP, Proteintech, USA; 1:1000).

Western Blot Analysis

At the indicated time points, the chondrocytes were washed twice with ice-cold PBS and collected in RIPA buffer (cat. No. ab156034; Abcam, UK) containing a protease inhibitor cocktail (cat. No. TAAR-BBI2; BIOTOOLS, Taiwan), and the lysates were cleared by centrifugation at 14,000 rpm for 15 min at 4°C. Total protein was quantified via a BCA protein assay kit (cat. No. 23225, Thermo Scientific, USA), and 25–35 μg/mL per sample was used for Western blotting. Proteins were separated by SDS–PAGE at 120 V for 3 h and transferred to PVDF membranes. To accommodate multiple targets and to avoid signal loss from repeated stripping and reprobing, membranes were wrapped in plastic film and horizontally sectioned at approximately 70 kDa and 35 kDa after transfer. This allowed the upper and lower membrane portions to be probed independently for different proteins. The splice-like appearance in the housekeeper western band resulted from this routine membrane-sectioning procedure. The membranes were blocked in 5% BSA at room temperature for 1 h and then incubated overnight with the appropriate primary antibodies. The membranes were then incubated with an HRP-

conjugated secondary antibody [goat anti-rabbit IgG (H+L) (cat. No. C04003, Croyez Bioscience Co., Ltd., Taiwan); 1:5000, goat anti-mouse IgG (cat. No. C04001, Croyez Bioscience Co., Ltd., Taiwan); 1:5000] for 2 h at room temperature. The bands were detected with SuperSignal™ West Pico PLUS Chemiluminescent Substrate (cat. No. 34580; Thermo Scientific, USA), and the band intensity was quantified using a FUSION-FX imaging system (Vilber Lourmat, Collégien, France).

ELISA

At the indicated points, the culture medium of the chondrocytes was collected and centrifuged for ELISAs. The protein concentrations of Col-I [human collagen type I alpha 1 ELISA kit (COL1a1), cat. No. RK01149, ABclonal,China] and Col-II [human collagen type II alpha 1 ELISA kit (COL2a1), cat. No. RK01152, ABclonal, China] synthesised by chondrocytes were determined using ELISA kits. All tests were performed according to the manufacturer's instructions. The absorbance was measured at 450 nm using an automatic enzyme labelling instrument. For normalisation, the DNA concentration was measured using a Quant-iT Picogreen dsDNA Assay Kit (cat. No. P7589, Invitrogen, USA).

Immunohistochemistry (IHC)

For IHC staining, the chondrocytes were fixed with 4% paraformaldehyde and then treated with 1.0% Triton 100. Chondrocytes were blocked with 0.1% BSA in PBS for 30 min and then incubated overnight at 4°C with primary antibodies against Col-II (cat. No. ab34712, Abcam, UK; 1:100), Col-I (cat. No. ab34710, Abcam, UK; 1:100), and SOD-2 (cat. No. 24127-1-AP, Proteintech, USA; 1:100). Afterwards, the sections were washed and incubated with secondary antibody [goat anti-rabbit IgG H&L (Alexa Fluor); cat. No. ab150077; Abcam, UK; 1:200] for 1 h and then washed. After counterstaining with DAPI, the slides were washed with PBS 3 times and coverslipped. IHC staining images were captured using a fluorescence microscope (Invitrogen, EVOS M7000).

Statistical Analysis

The data are expressed as the means ± standard errors of the means (SEM) of the combined data of the experimental replicates. The statistical significance was evaluated using a one-way analysis of variance (ANOVA), and multiple comparisons were performed using Scheffe's method. $p < 0.05$ was considered significant.

Results

Increased Oxidative Stress and Mitochondrial Dysfunction are Associated with Enhanced Mitochondrial Oxidative Phosphorylation in Chondrocytes After Monolayer Expansion in vitro

To assess whether monolayer expansion *in vitro* alters mitochondrial energy metabolism in chondrocytes, we analysed both non-mitochondrial (glycolytic) and mitochondrial (oxidative phosphorylation) metabolism in chondrocytes from the C and ME groups. The results revealed increased oxidative phosphorylation in chondrocytes after monolayer expansion *in vitro*. The ECAR of the chondrocytes did not differ between the C and ME groups (Fig. 1**a**). Compared with that of the chondrocytes in the C group, the OCR of the chondrocytes in the ME group was greater (Fig. 1**b**).

Since monolayer expansion *in vitro* increased oxidative phosphorylation of mitochondria in chondrocytes, we further investigated whether oxidative stress and mitochondrial dysfunction are accompanied by increased OCR of chondrocytes. We assessed mitochondrial ROS production, 8-OHdG levels, the MMP, mitochondrial mass, and the level of PGC-1α in chondrocytes. Increased mitochondrial ROS production in chondrocytes after monolayer expansion *in vitro* was detected. More intense MitoSOX staining was found in the chondrocytes in the ME group than in those in the C group (Fig. 1**c**). The quantitative results of MitoSOX staining also revealed a significant increase in mitochondrial ROS production by chondrocytes in the ME group compared with the C group (Fig. 1**d**). 8-OHdG is a marker of oxidative stress [49]. Compared with those in the C group, increased levels of 8-OHdG in the chondrocytes in the ME group were found (Fig. 1**e**). These results indicate that increased oxidative stress is accompanied by increased OCR of chondrocytes.

Mitochondrial dysfunction is also found in chondrocytes after monolayer expansion *in vitro*. Compared with that in the C group, decreased MMP was detected in chondrocytes in the ME group (Fig. 1**f**). Increased mitochondrial mass in chondrocytes were observed after monolayer expansion *in vitro*. The mitochondria stained with MitoSpy revealed that the ME group displays higher fluorescence staining area compared to the C group, suggesting higher mitochondrial mass (Fig. 1**g** and **h**). Moreover, the protein expression of PGC-1α was lower in the chondrocytes in the ME group than in those in the C group, indicating that the biogenesis of mitochondria was decreased (Fig. 1**i** and **j**). Overall, these results indicate that oxidative stress and mitochondrial dysfunction are accompanied by increased oxidative phosphorylation of mitochondria in chondrocytes after monolayer expansion *in vitro*.

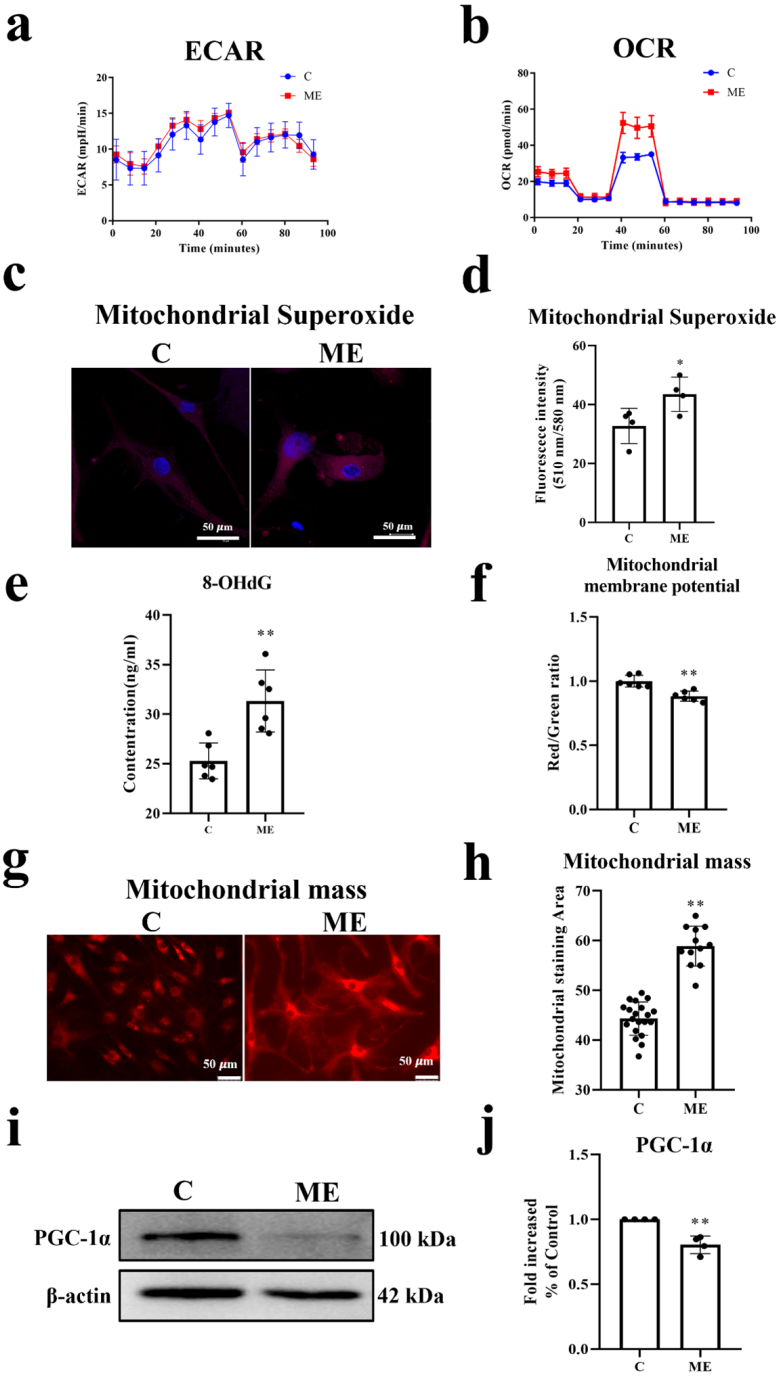

Fig. 1. Increased oxidative stress and mitochondrial dysfunction are associated with enhanced mitochondrial oxidative phosphorylation in chondrocytes after monolayer expansion *in vitro*. The mitochondrial energy metabolism, mitochondrial superoxide level, oxidative stress, MMP, mitochondrial mass and protein level of PGC-1α in chondrocytes in the C and ME groups were analysed. (**a**) ECAR and (**b**) OCR were determined with a Seahorse XFe 24 Analyzer. (**c**) The confocal microscopic images of chondrocytes stained with MitoSOX Red (red) for mitochondrial superoxide; the cell nuclei were stained with DAPI (blue). (**d**) Mitochondrial superoxide production was quantified by the fluorescence intensity of MitoSOX Red staining (n = 4). Scale bar = 50 μm. (**e**) Quantification of 8-OHdG production in chondrocytes (n = 6). **(f)** MMP was examined by JC-10 (n = 6). The ratio of the intensities of the red and green fluorescence is expressed relative to that of the C group, which was defined as 1. (**g**) Representative fluorescence microscopy images of chondrocytes stained with MitoSpy (Red) to evaluate mitochondrial mass. Scale bar = 50 μm. (**h**) Mitochondrial mass was quantified by the fluorescence area of MitoSpy staining. (**i**) The protein levels of PGC-1α and β-actin in chondrocytes were analysed by Western blotting, and representative immunoblots are shown. (**j**) Quantification of PGC-1α protein expression was performed by densitometric analysis, with all values normalized to β-actin and expressed relative to the C group, which was defined as 1. The data are presented as the means $\pm$ SEMs (n = 4). (*) and (**) indicate $p < 0.05$ and $p < 0.01$, respectively, compared with the chondrocytes in the C group.

Isolation of Mitochondria From ADSC and ADSC-MT Into Chondrocytes

COX IV is a marker for mitochondrial organelles and is one of the subunits of cytochrome C oxidase in the inner mitochondrial membrane [50]. VDAC-1 is the most abundant protein on the outer membrane of mitochondria [51]. To confirm that mitochondria were isolated from ADSC, we determined the protein levels of COX IV, VDAC-1 and α-tubulin in ADSC and isolated mitochondria by Western blot analysis. The protein levels of COX IV and VDAC-1 were abundant in both ADSC and mitochondria isolated from ADSC (ADSC-mitochondria) (Fig. 2**a**). However, the protein level of α-tubulin was low in ADSC-mitochondria (Fig. 2**a**). These results indicate that the mitochondria were successfully isolated from ADSC.

For ADSC-MT in chondrocytes, freshly isolated MitoSpy-labelled ADSC mitochondria were immediately cocultured with chondrocytes. To confirm that mitochondria were successfully taken up by chondrocytes after ADSC-MT, we assessed the uptake of MitoSpy-labelled ADSC-mitochondria by chondrocytes under a fluorescence microscope at 1h and days 1–3. One hour after ADSC-MT, the MitoSpy-labelled ADSC mitochondria were visualized in the cytoplasm of the chondrocytes (Fig. 2**b** and **c**). Moreover, MitoSpy-labelled ADSC mitochondria were still observable in chondrocytes from days 1 to 3 after ADSC-MT (Fig. 2**d** and **e**). Since VDAC-1 is the most abundant protein on the outer membrane of mitochondria [51], measuring its cellular expression may serve as an indicator of mitochondrial content within the cell. We further tested the protein level of VDAC-1 in chondrocytes 3 days after ADSC-MT and found that the protein level of VDAC-1 in the chondrocytes in the AM group was greater than that in the C group (Fig. 2**f** and **g**). This result suggests that the protein level of VDAC-1 in AM group is higher than that in the C and ME group due to the VDAC-1 expression in AM group is consist of mitochondria derived from chondrocytes and ADSC (Fig. 2**f** and **g**). Overall, the results indicated that ADSC mitochondria were isolated and successfully transferred into chondrocytes by ADSC-MT.

ADSC-MT Ameliorates Senescence in Senescent Chondrocytes

SA-β-gal is one of the first biomarkers described in cells with features of senescence [17]. Moreover, increased expression of p16 and p21 induces cell-cycle arrest in senescent cells by inhibiting cyclin-dependent kinases [13,52]. Chondrocytes exhibiting increased SA-β-gal staining along with elevated p16 and p21 expression demonstrate enhanced cellular senescence [13,52]. To determine whether ADSC-MT ameliorates senescence in senescent chondrocytes, the expression of senescence-associated markers, including SA-β-gal, and the protein levels of p16 and p21 in chondrocytes were analysed in the C, ME and AM groups. These results showed that ADSC-MT ameliorates senescence in senescent chondrocytes. SA-β-gal staining revealed that the chondrocytes in both the C and AM groups had more negatively stained areas than those in the ME group did (Fig. 3**a**). Quantitative analysis also revealed that both the C and AM groups exhibited a lower area of blue staining compared to the ME group (Fig. 3**b**). The senescence of chondrocytes in the three groups was further confirmed by determining the protein levels of p16 and p21 in chondrocytes. The results also revealed that the protein levels of p16 and p21 were markedly lower in the AM group than in the ME group (Fig. 3**c**–**f**). Overall, these results indicate that ADSC-MT attenuates chondrocyte senescence induced by monolayer expansion *in vitro*.

ADSC-MT Improves the Chondrogenic Phenotype of Senescent Chondrocytes

In addition to reducing senescence, improving the chondrogenic phenotype is critical for synthesizing hyaline cartilage in senescent chondrocytes. We next evaluated whether ADSC-MT improved the chondrogenic phenotype of senescent chondrocytes. To evaluate the chondrogenic phenotype of chondrocytes after ADSC-MT, we determined the mRNA levels of Col-II and Col-I in chondrocytes via RT–qPCR analyses on day 3 after ADSC-MT. The results showed that ADSC-MT into chondrocytes improved the chondrogenic phenotype of senescent chondrocytes. Compared with those in the C group, decreased Col-II and increased Col-I mRNA levels in chondrocytes were detected in the ME group (Fig. 4**a** and **b**). Compared with those in the ME group, the mRNA levels of Col-II and Col-I in the AM group were reversed (Fig. 4**a** and **b**). The Col-II/Col-I expression ratio was also calculated to assess chondrogenic potential. No significant difference was found between the C and AM groups (Fig. 4**c**). The results showed that ADSC-MT treatment improved the chondrogenic potential of senescent chondrocytes. To confirm the results at the mRNA level, we further evaluated the protein levels of Col-II and Col-I in chondrocytes via ELISAs and IHC staining on day 12 after ADSC-MT. Similar results were found via ELISAs, with decreased Col-II and increased Col-I synthesis in the ME group compared with those in the C group. These changes were also reversed in the AM group compared with those in the ME group (Fig. 4**d** and **e**). No significant difference in the Col-II/Col-I expression ratio was observed between the C and AM groups (Fig. 4**f**). The same results were also found via IHC staining of Col-II and Col-I in chondrocytes (Fig. 4**g**). Collectively, these results indicate that ADSC-MT improves the chondrogenic phenotype of senescent chondrocytes, even after monolayer expansion *in vitro*.

ADSC-MT Reduces Oxidative Stress and Mitochondrial Dysfunction in Senescent Chondrocytes

Since we found that ADSC-MT reduces senescence and improves the chondrogenic phenotype of senescent

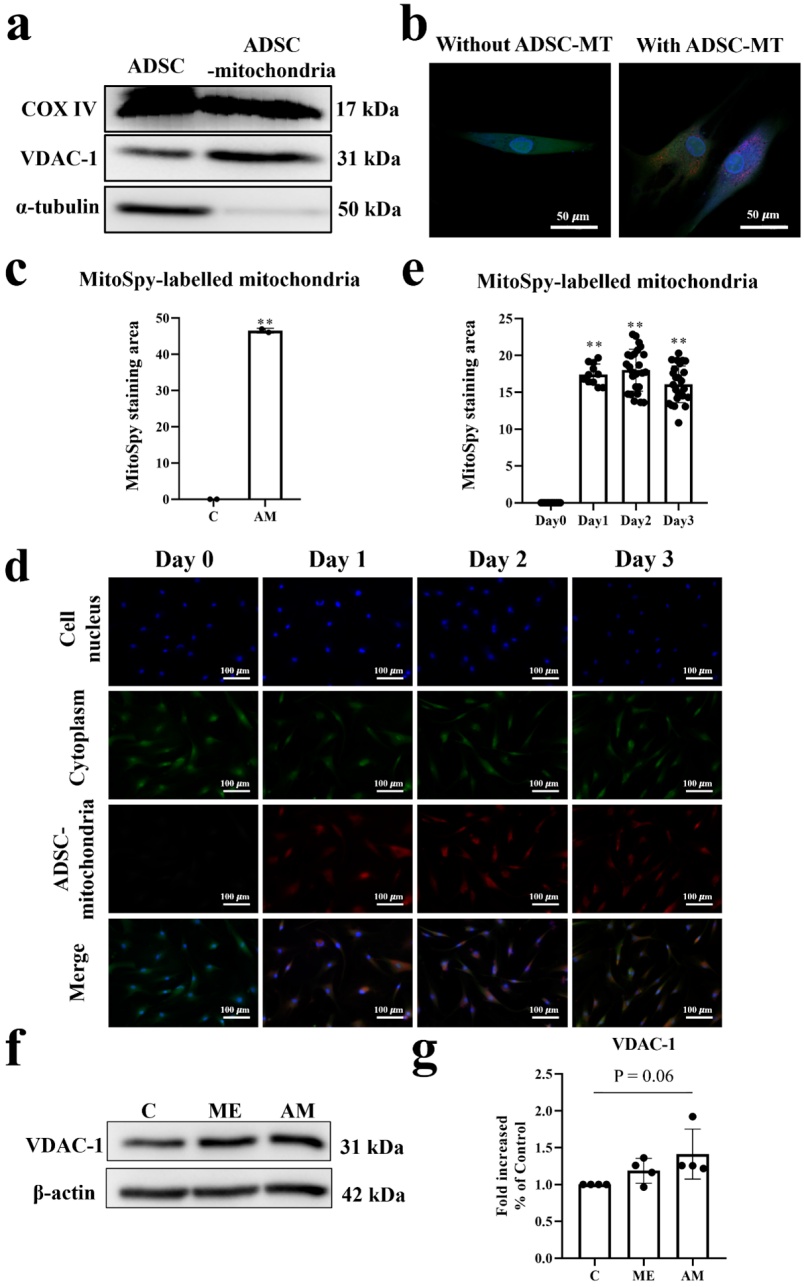

Fig. 2. Isolation of mitochondria from ADSC and ADSC-MT into chondrocytes. MitoSpy-labelled mitochondria were freshly isolated from ADSC (ADSC mitochondria) and transferred into chondrocytes via ADSC-MT. (**a**) Western blot analysis of COX IV, VDAC-1 and α-tubulin in ADSC and in ADSC mitochondria. (**b**) Confocal microscopic images of chondrocytes treated with or without ADSC-MT after 1 h. ADSC mitochondria were stained with MitoSpy (red), the chondrocyte cytoplasm was stained with CellTracker Green CMFDA (green), and the cell nuclei were stained with DAPI (blue). Scale bar = 50 µm. (**c**) ADSC mitochondria were quantified based on the fluorescence area obtained from MitoSpy staining. (**d**) Representative confocal microscopic images of chondrocytes that received ADSC-MT from days 0 to 3. ADSC mitochondria were previously labelled with MitoSpy (red), and the chondrocyte cytoplasm and cell nucleus were labelled with CellTracker Green CMFDA (green) and DAPI (blue), respectively. Scale bar = 100 μm. (**e**) ADSC mitochondria were quantified based on the fluorescence area obtained from MitoSpy staining. (**f**) The protein levels of VDAC-1 and β-actin in chondrocytes in the C, ME and AM groups were analysed by Western blotting, and representative immunoblots are shown. (**g**) Quantification of VDAC-1 and β-actin protein expressions were performed by densitometric analysis, with all values normalized to β-actin and expressed relative to the C group, which was defined as 1. The data are presented as the means ± SEMs (n = 4). (**) $p <$ 0.01, respectively, compared with the chondrocytes in the C group.

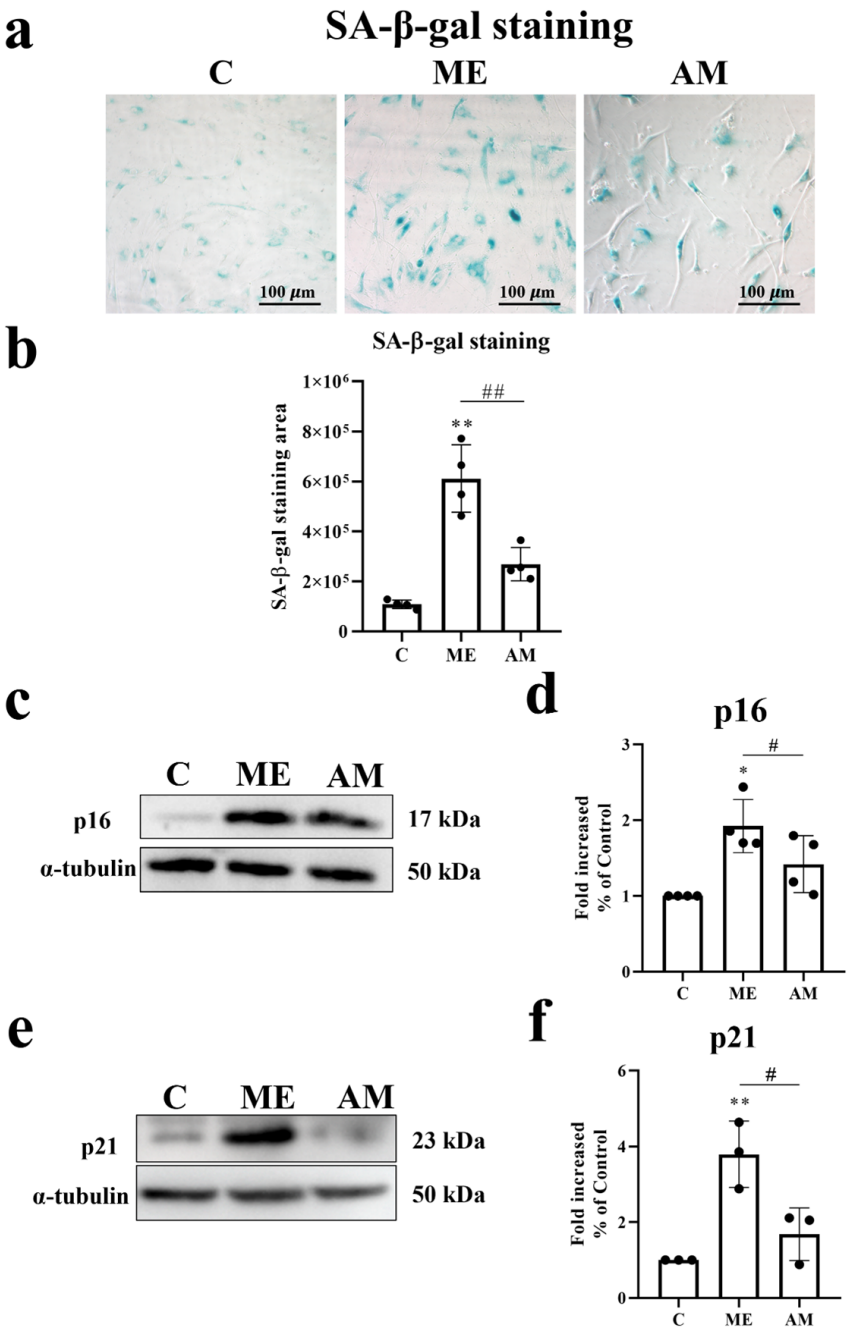

Fig. 3. ADSC-MT ameliorates senescence in senescent chondrocytes. The cell senescence of chondrocytes in the C, ME and AM groups was analysed. (**a**) SA-β-gal staining (blue) of chondrocytes. Scale bar = 100 μm. (**b**) Quantitative analysis of blue staining intensity of chondrocytes in three groups. (**c**) The protein levels of p16 and α-tubulin in chondrocytes were analysed by Western blotting, and representative immunoblots are shown. (**d**) Quantification of p16 and α-tubulin protein expressions were performed by densitometric analysis, with all values normalized to α-tubulin and expressed relative to the C group, which was defined as 1. (**e**) The protein levels of p21 and α-tubulin in chondrocytes were analysed by Western blotting, and representative immunoblots are shown. (**f**) Quantification of p21 and α-tubulin protein expressions were performed by densitometric analysis, with all values normalized to α-tubulin and expressed relative to the C group, which was defined as 1. The data are presented as the means $\pm$ SEMs (n = 3–4). (*) and (**) indicate $p < 0.05$ and $p < 0.01$, respectively, compared with the chondrocytes in the C group. (#) $p < 0.05$, (##) $p < 0.01$, compared with the ME group.

chondrocytes, we further tested whether this effect occurs via reduced oxidative stress and mitochondrial dysfunction in chondrocytes. We observed reduced oxidative stress in chondrocytes after ADSC-MT. First, mitochondrial superoxide synthesis in chondrocytes decreased after ADSC-MT. Compared with that in the C group, mitochondrial superoxide synthesis in chondrocytes increased in the ME group (Fig. 5**a**). This synthesis was lower in the AM group than

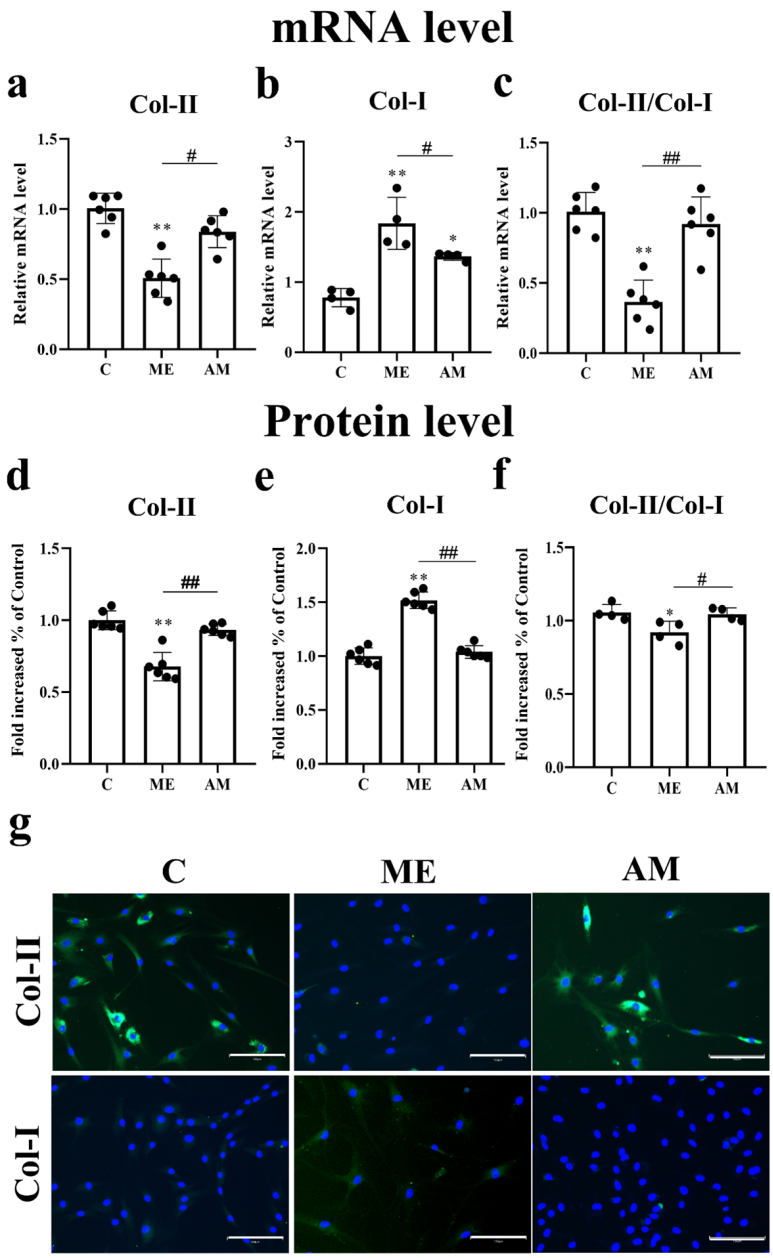

Fig. 4. ADSC-MT improves the chondrogenic phenotype of senescent chondrocytes. The chondrogenic phenotypes of the chondrocytes in the C, ME and AM groups were analysed. The mRNA expression levels of (**a**) Col-II and (**b**) Col-I in chondrocytes in the 3 groups were measured on day 3. (**c**) The Col-II/Col-I expression ratio was also calculated to assess chondrogenic potential. Gene expression levels are expressed relative to those in the C group, which was defined as 1. ELISAs were used to determine the protein levels of (**d**) Col-II and (**e**) Col-I in the chondrocytes of the 3 groups on day 12. (**f**) The Col-II/Col-I protein ratio was also calculated to evaluate the chondrogenic phenotype. Protein expression levels are expressed relative to those in the C group, which was defined as 1. The values are presented as the mean ± SEM (n = 4). (*) and (**) indicate $p < 0.05$ and $p < 0.01$, respectively, compared with the C group. (#) $p < 0.05$, (##) $p < 0.01$, compared with the ME group. (**g**) IHC staining of Col-II and Col-I in chondrocytes from the 3 groups on day 12. The IHC images of chondrocytes stained with Col-II (green) or Col-I (green); the cell nuclei were stained with DAPI (blue). Scale bar = 150 μm.

in the ME group (Fig. 5**a**). Second, ADSC-MT also decreases the level of 8-OHdG in chondrocytes. The increase in 8-OHdG found in the chondrocytes in the ME group was reversed in the AM group (Fig. 5**b**). Moreover, mitochondrial dysfunction in monolayer-expanded chondrocytes was reduced. Compared with that in the C group, the decreased MMP in chondrocytes in the ME group was reversed in the cells in the AM group (Fig. 5**c**).

We also analysed the change in mitochondrial energy metabolism in chondrocytes after ADSC-MT. We found

that ADSC-MT did not affect glycolysis or oxidative phosphorylation in chondrocytes after monolayer expansion *in vitro*. Glycolysis and oxidative phosphorylation did not differ between the ME and AM groups (Fig. 5**d** and **e**). Overall, these results indicate that ADSC-MT reduces oxidative stress and mitochondrial dysfunction in senescent chondrocytes.

ADSC-MT Increases the Antioxidant Defence Capacity and Mitochondrial Biogenesis of MQC in Senescent Chondrocytes

To test the antioxidant defence capacity and mitochondrial biogenesis of chondrocytes after ADSC-MT, we determined the protein levels of SOD-2, SIRT-1, SIRT-3, PGC-1α, and transcription factor A (TFAM) in chondrocytes in the three groups. These results showed that ADSC-MT promotes the antioxidant defence capacity of senescent chondrocytes. Compared with those in the C and ME groups, the protein level of SOD-2 in chondrocytes in the AM group was increased (Fig. 6**a** and **b**). More intense fluorescence of SOD-2 in chondrocytes in the AM group was also detected via IHC staining (Fig. 6**c**). Compared with those in the ME group, the protein levels of SIRT-1, SIRT-3, PGC-1α, and TFAM in chondrocytes were increased in the AM group, indicating increased mitochondrial biogenesis in chondrocytes after ADSC-MT (Fig. 6**d**–**k**). The results showed that ADSC-MT increases both the antioxidant defence capacity and mitochondrial biogenesis of MQC in senescent chondrocytes.

ADSC-MT Does Not Change Mitochondrial Dynamics But Promotes Mitophagy in Senescent Chondrocytes

To test the mitochondrial dynamics and mitophagy of chondrocytes after ADSC-MT, we determined the protein levels of MFN-1, MFN-2, OPA-1, PINK-1 and Parkin in chondrocytes in the three groups. We found that ADSC-MT does not affect mitochondrial dynamics in senescent chondrocytes. Compared with those in the ME group, the protein levels of MFN-1, MFN-2, and OPA-1 were not different in the AM group (Fig. 7**a**–**d**). Thus, ADSC-MT promotes mitophagy in senescent chondrocytes. Compared with those in the ME group, the protein levels of PINK-1 and Parkin in chondrocytes were lower in the AM group (Fig. 7**e**–**g**). The results showed that ADSC-MT does not affect mitochondrial dynamics but increases mitophagy in senescent chondrocytes.

Discussion

When sufficient chondrocytes are obtained via monolayer expansion *in vitro* for articular cartilage tissue engineering, the chondrocytes undergo rapid senescence and lose their chondrogenic phenotype [10]. The senescence of chondrocytes results in the formation of undesired fibrocartilage at the transplantation site [8,16]. For the regeneration of articular cartilage defects in the clinic, chondrocyte senescence remains the major barrier in chondrocyte-based articular cartilage tissue engineering. For example, autologous chondrocyte implantation (ACI) has been used for more than 30 years in the clinic and is still considered the gold standard for treating articular cartilage defects [53,54]. However, chondrocytes lose their chondrogenic phenotype after monolayer expansion *in vitro*, which impairs their ability to synthesize hyaline cartilage [4,13]. In this study, we show that ADSC-MT improves the chondrogenic phenotype of senescent chondrocytes by ameliorating mitochondrial dysfunction, suggesting that ADSC-MT may be a strategy for chondrocyte-based articular cartilage tissue engineering.

Previous studies have shown an increased oxidative phosphorylation rate of mitochondria with concomitant mitochondrial ROS production and oxidative stress in chondrocytes after monolayer expansion *in vitro* [21,22]. Superoxide is a proximal mitochondrial ROS that is produced at respiratory chain complexes I and III [18,35]. 8-OHdG is a product of oxidative modifications of DNA and is a marker of oxidative stress [49]. Consistent with these previous reports, our results also revealed increased oxidative phosphorylation rates in mitochondria with increased mitochondrial ROS production and 8-OHdG in chondrocytes after monolayer expansion *in vitro* (Fig. 1**b**–**e**). These results suggest that enhanced mitochondrial oxidative phosphorylation in chondrocytes following *in vitro* monolayer expansion is associated with increased oxidative stress.

Chondrocyte senescence occurs after monolayer expansion *in vitro* [13,52]. Increased oxidative stress is known to cause cell senescence, which has been linked to the development of mitochondrial dysfunction [13,17,18]. In chondrocytes, oxidative stress can lead to senescence and mitochondrial dysfunction [13,55]. Senescent cells are characterized by changes in mitochondrial mass and the MMP [17]. Mitochondrial mass is often increased in senescence *in vitro* [56]. Previous studies have reported that senescent fibroblasts exhibit greater mitochondrial mass and lower MMP compared to non-senescent cells [56]. Moreover, a decrease in mitochondrial biogenesis is a characteristic of mitochondrial dysfunction [57,58]. PGC-1α plays an important role in the regulation of mitochondrial biogenesis and function [18,35]. Our results also revealed a decreased MMP, increased mitochondrial mass, and decreased PGC-1α expression in chondrocytes after monolayer expansion *in vitro* (Fig. 1**f**–**j**). These results suggest that increased oxidative stress in chondrocytes after monolayer expansion *in vitro* leads to senescence and mitochondrial dysfunction.

MT is a process by which mitochondria are transferred from one cell to another [59]. MT has been shown to reduce oxidative stress and normalise mitochondrial function in cells [59]. Recent studies have shown that MSCs also exert their biological effects through MT [60]. Recipient cells of mitochondria from MSCs show normalised mito-

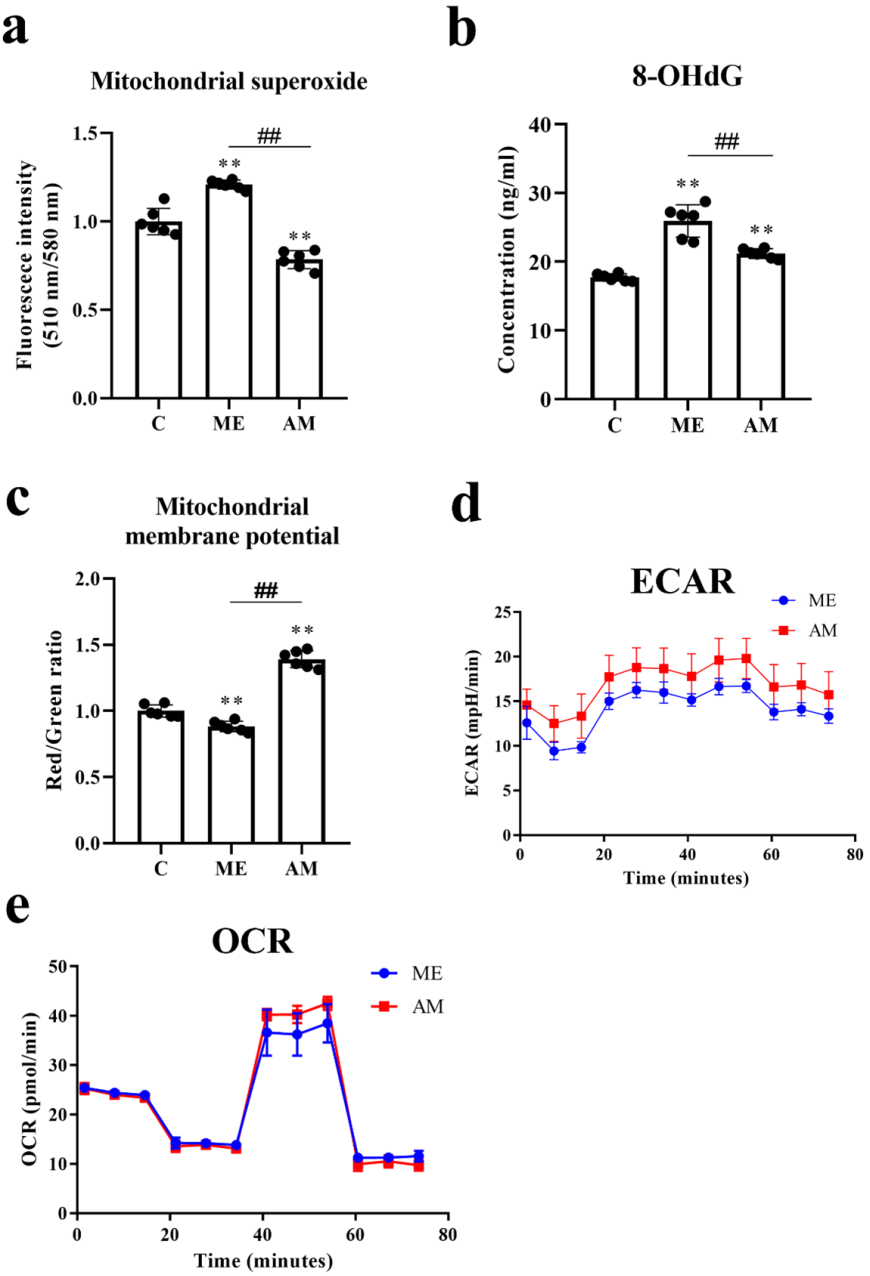

Fig. 5. ADSC-MT reduces oxidative stress and mitochondrial dysfunction in senescent chondrocytes. The mitochondrial superoxide levels, oxidative stress, MMP, and mitochondrial energy metabolism of the chondrocytes in the C, ME and AM groups were analysed. (**a**) Mitochondrial superoxide production was determined by quantifying the intensity of MitoSOX Red staining (n = 6). (**b**) Quantification of 8-OHdG production in chondrocytes (n = 6). (**c**) MMP was examined by JC-10 (n = 6). The intensity of the fluorescence of JC-10 is expressed relative to that of the C group, which was defined as 1. The values are presented as the means ± SEMs. (**) $p < 0.01$, respectively, compared with the C group. (##) $p < 0.01$, compared with the ME group. (**d**) ECAR was determined with a Seahorse XFe 24 Analyser. (**e**) OCRs were determined with a Seahorse XFe 24 Analyser.

chondrial function, such as resistance to oxidative stress and increased MMP [61,62]. Moreover, oxidative stress (or overproduction of ROS) is considered a major regulator of chondrocyte senescence, which is responsible for the loss of the chondrogenic phenotype after monolayer expansion *in vitro* [13]. In addition, a previous report showed that isolated mitochondria can be artificially transferred *in vitro* into cells by simple coincubation of isolated mitochondria with cells without the need for transfection reagents, supplements to the medium or any other type of intervention [63]. In this study, we showed that ADSC mitochondria were transferred into recipient chondrocytes by coincubation of isolated mitochondria with cells (Fig. 2). We found that senescent chondrocytes that received ADSC-MT ex-

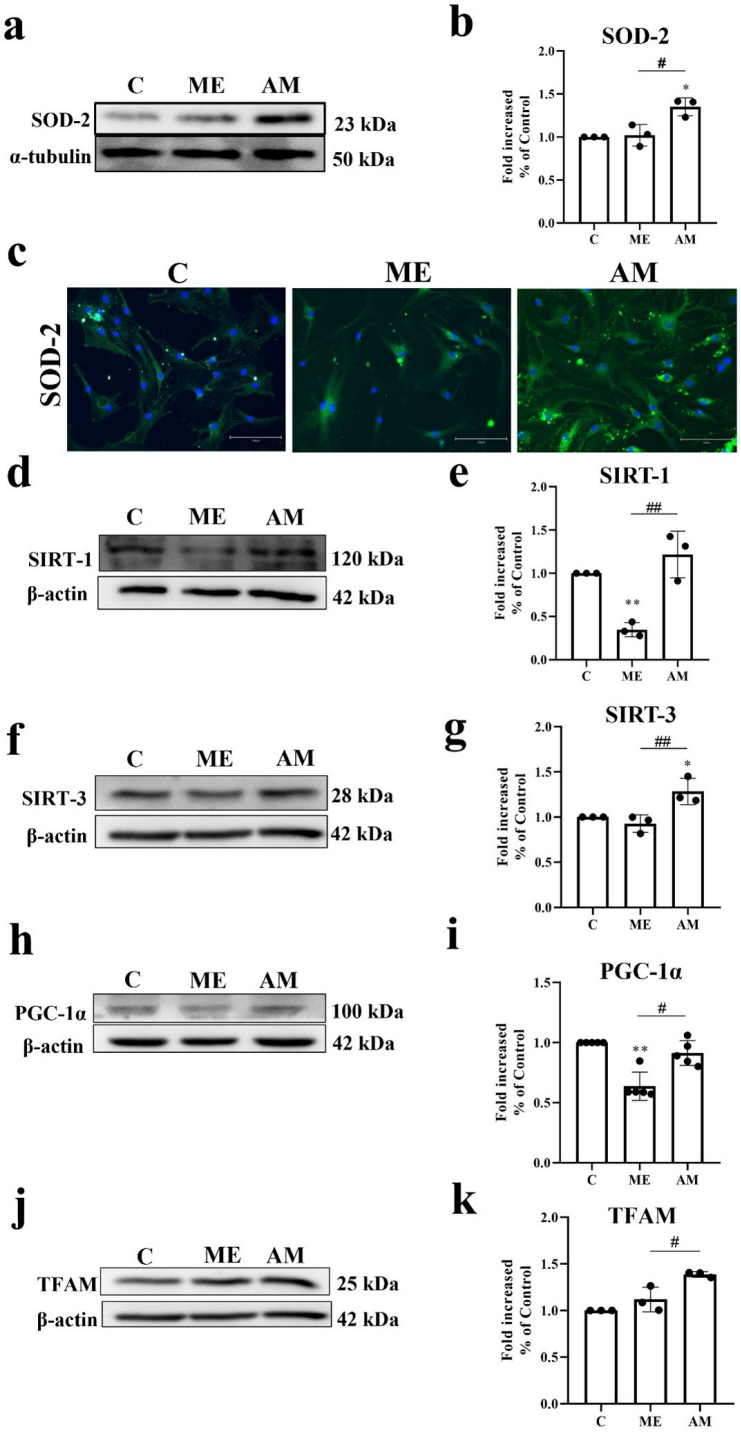

Fig. 6. ADSC-MT promotes antioxidant defence capacity and mitochondrial biogenesis in senescent chondrocytes. The protein levels of SOD-2, SIRT-1, SIRT-3, PGC-1α, and TFAM in chondrocytes in the C, ME and AM groups were analysed. (**a**) The protein expression levels of SOD-2 and α-tubulin in chondrocytes were detected by Western blotting, and representative immunoblots are shown. (**b**) Quantification of SOD-2 and α-tubulin protein expressions were performed by densitometric analysis, with all values normalized to α-tubulin and expressed relative to the C group, which was defined as 1. (**c**) The IHC images of chondrocytes were stained with SOD-2 (green fluorescence), and the cell nuclei were stained with DAPI (blue). Scale bar = 150 μm. The protein expression levels of (**d**) SIRT-1, (**f**) SIRT-3, (**h**) PGC-1α, (**j**) TFAM and β-actin in chondrocytes were determined by Western blotting, and representative immunoblots are shown. Quantification of **(e)** SIRT-1, (**g**) SIRT-3, (**i**) PGC-1α, (**k**) TFAM and β-actin protein expressions were performed by densitometric analysis, with all values normalized to β-actin and expressed relative to the C group, which was defined as 1. The data are presented as the means ± SEMs (n = 3–5). (*) and (**) indicate $p < 0.05$ and $p < 0.01$, respectively, compared with the chondrocytes in the C group. (#) and (##) indicate $p < 0.05$ and p < 0.01, respectively, compared with the ME group.

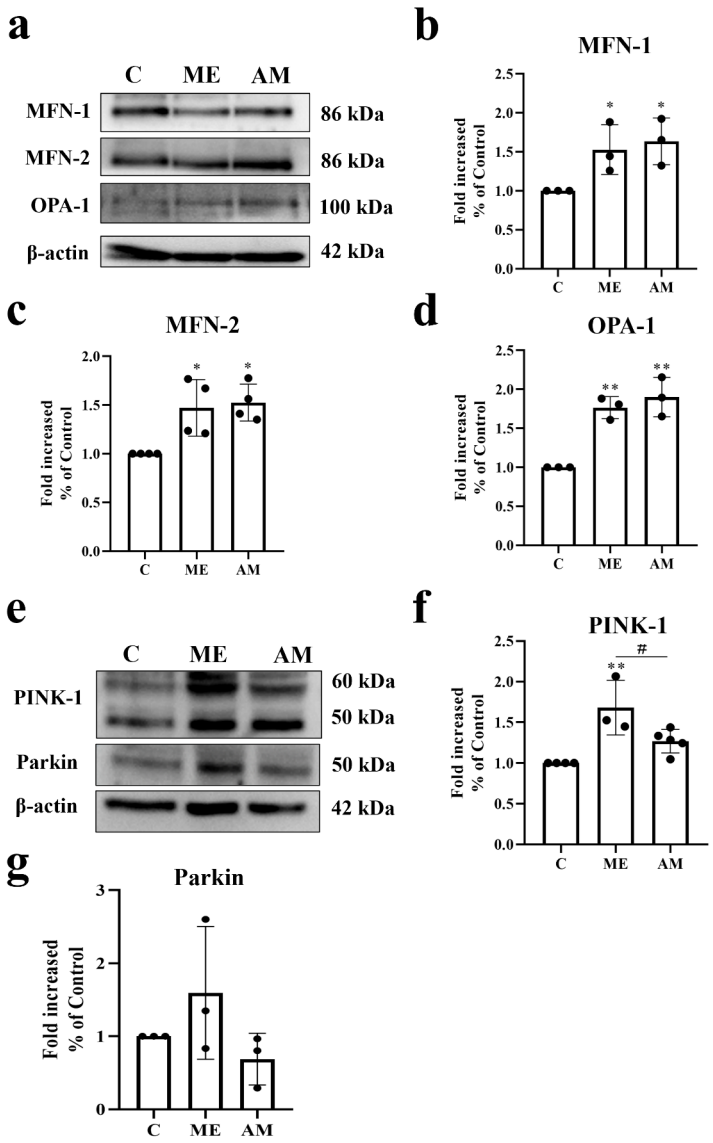

Fig. 7. ADSC-MT does not change mitochondrial dynamics but increases mitophagy in senescent chondrocytes. The protein levels of MFN-1, MFN-2, OPA-1, PINK-1, and Parkin in the chondrocytes in the C, ME and AM groups were analysed. The protein expression levels of (**a**) MFN-1, MFN-2, OPA-1, (**e**) PINK-1, Parkin and β-actin in chondrocytes were determined by Western blotting, and representative immunoblots are shown. Quantification of **(b)** MFN-1, (**c**) MFN-2, (**d**) OPA-1, (**f**) PINK-1, (**g**) Parkin and β-actin protein expressions were performed by densitometric analysis, with all values normalized to β-actin and expressed relative to the C group, which was defined as 1. The data are presented as the means ± SEMs (n = 3–5). (*) and (**) indicate $p < 0.05$ and $p < 0.01$, respectively, compared with the chondrocytes in the C group. (#) indicates $p < 0.05$, compared with the ME group.

hibited alleviated senescence and a restored chondrogenic phenotype (Fig. 3 and 4). ADSC-MT reduced the intensity of SA-β-gal staining and the protein levels of p21 and p16 in senescent chondrocytes (Fig. 3). ADSC-MT increases the expression of Col-II and decreases the expression of Col-I in senescent chondrocytes at both the mRNA and protein levels (Fig. 4). Moreover, we found that ADSC-MT alleviated mitochondrial dysfunction in senescent chondrocytes by reducing oxidative stress and increasing the MMP (Fig. 5). ADSC-MT decreased the production of mitochondrial superoxide and the level of 8-OHdG in senescent chondrocytes (Fig. 5**a** and **b**). In addition, ADSC-MT increased the MMP in senescent chondrocytes (Fig. 5**c**). These results suggest that ADSC-MT improves the chondrogenic phenotype in senescent chondrocytes by ameliorating mitochondrial dysfunction.

MQC is vital for maintaining the normal functions of mitochondria and operates through the coordination of various processes to maintain cell function [18,35]. The primary function of MQC is to ensure mitochondrial quality and maintain mitochondrial functions by limiting oxidative damage to mitochondria [18]. The known mecha-

nisms linking MQC to regulate cell function in chondrocytes include antioxidant defences, mitochondrial biogenesis, mitochondrial dynamics and mitophagy [35]. Mitochondria are major sources and targets of ROS, and excessive accumulation of ROS can lead to oxidative stress and cellular damage [18,35]. Superoxide is the main undesired by-product of mitochondrial oxidative phosphorylation. Superoxide is a mitochondrial ROS produced at respiratory chain complexes I and III [18,35]. The antioxidant system counteracts the detrimental effects of excessive ROS accumulation. SOD-2 acts as the first defence by converting superoxide into hydrogen peroxide. Catalase and glutathione peroxidase help remove hydrogen peroxide by turning it into water and oxygen [18,35]. Moreover, depletion of mitochondrially localised SOD-2 has been shown to promote mitochondrial dysfunction and increase ROS production [64,65]. We showed that ADSC-MT in chondrocytes decreased the level of mitochondrial ROS (Fig. 5**a**) and increased the protein level of SOD-2 (Fig. 6**a** and **b**). These results suggest that ADSC-MT alleviates mitochondrial dysfunction by promoting antioxidant defences in senescent chondrocytes.

Mitochondrial biogenesis is a process that leads to the replication of mitochondria, which play crucial roles in sustaining cell function by ensuring a continuous supply of new mitochondria [18,35]. PGC-1α plays an important role in the regulation of mitochondrial biogenesis and function [18,35]. In addition to PGC-1α, mitochondrial TFAM, through its binding to mtDNA, has been identified as a relevant modulator of mitochondrial biogenesis, including mtDNA transcription, maintenance, replication and mtDNA repair [18,35]. SIRT-1 is known to be responsible for the activation of PGC-1α [18,35]. SIRT-3 can deacetylate liver kinase B1 (LKB1), which can increase the level of PGC-1α [18,35]. We also showed that ADSC-MT increased the protein levels of SIRT-1, SIRT-3, PGC-1α, and TFAM in monolayer-expanded chondrocytes (Fig. 6**d**–**k**). These results suggest that ADSC-MT alleviates mitochondrial dysfunction by promoting mitochondrial biogenesis in senescent chondrocytes.

Mitochondrial dynamics involves the balance between fusion and fission and helps regulate the function of mitochondria. These processes play crucial roles in maintaining mitochondrial health and cellular function. The key proteins involved in mitochondrial fusion include MFN-1, MFN-2 and OPA-1. SIRT-3 plays a role in regulating the deacetylation status of OPA-1, which has a direct effect on mitochondrial dynamics [18,35]. Our results revealed that the levels of MFN-1, MFN-2 and OPA-1 were not altered in ADSC-MT recipient chondrocytes compared with those in senescent chondrocytes (Fig. 7**a**–**d**). Mitochondrial dynamics are known to contribute to mitochondrial respiration [66]. It has been reported that cells lacking MFN-1 and MFN-2 exhibit fragmented mitochondria, which is associated with reduced mitochondrial respiration [66–68]. Moreover, OPA1-deficient cells display fragmented mitochondria and diminished oxidative phosphorylation (OXPHOS) [69,70], whereas OPA-1 overexpression enhances OXPHOS [66,71]. In Fig. 5**e**, we observed that the OCR in senescent chondrocytes (ME group) remains unchanged after ADSC-MT treatment (AM group). We suggest that OCR does not differ between these two groups (Fig. 5**e**) which may explain why the upregulation of MFN-1, MFN-2, and OPA-1 in both the ME and AM groups (Fig. 7**a**–**d**). However, the detailed molecular mechanism still requires further investigation.

The upregulation of PINK-1 and Parkin constitutes a conserved cellular defence mechanism in response to mitochondrial damage, initiating mitophagy—a selective autophagic process that facilitates the targeted degradation of dysfunctional or superfluous mitochondria, thereby preserving mitochondrial quality and cellular homeostasis [18,35,72]. Parkin, an E3 ubiquitin ligase and mitochondrial outer membrane (OMM) protein, operates in conjunction with PINK-1, and phosphorylation of Parkin by PINK-1 transforms it into an active phospho-ubiquitin dependent E3 ligase, which can respond to the loss of MMP to eliminate damaged mitochondria [73]. It has been shown that Parkin-mediated clearance of damaged mitochondria limits the generation of ROS and prevents the induction of oxidative stress in chondrocytes [74]. Our results show elevated PINK-1 and Parkin levels in ME group chondrocytes compared to C group, which were reversed in the AM group (Fig. 7**e**–**g**). These results suggest that damaged mitochondria accumulated in senescent chondrocytes are reduced following ADSC-MT treatment. Furthermore, the loss of MMP and elevated oxidative stress are also alleviated in senescent chondrocytes after ADSC-MT. However, the expression levels of PINK-1 and Parkin alone are insufficient to determine whether mitophagy is actively occurring. To determine whether mitophagy is activated or inhibited in senescent chondrocytes after ADSC-MT treatment, the LC3-I/LC3-II ratio and the protein expression of p62/SQSTM1 should be measured in the future. Overall, these results suggest that ADSC-MT reduces the degree of mitochondrial dysfunction in senescent chondrocytes by promoting MQC in chondrocytes.

In the ME group, decreased PGC-1α (Fig. 1**i**) and increased ROS (Fig. 1**c** and **d**) would suggest VDAC-1 activation; however, VDAC-1 expression was not significantly upregulated (Fig. 2**f** and **g**). It has been indicated that VDAC-1 expression is regulated by the AMPK/PGC-1α and p53 pathways in neural cells [75]. Not only AMPK/PGC-1α signaling pathway modulates VDAC-1 expression, but also VDAC-1 expression is regulated by p53. Silencing of p53 suppresses VDAC-1 expression, whereas its overexpression enhances VDAC-1 transcription and expression, with identified p53 binding sites on the VDAC-1 promoter [75]. In our unpublished data, we also find that the protein level of p53 in chondrocytes is not

changed in the C and ME groups. Based on the described above, we suggest that the expression of VDAC-1 in chondrocytes is not altered in the ME group compared to the C group, as the protein levels of p53 in chondrocytes remain unchanged between the two groups.

MMP is a measure of the charge difference across the inner mitochondrial membrane, and it is closely linked to ROS production. Mitochondria are both a major source and target of ROS due to their aerobic metabolism. High ROS can damage mitochondrial DNA and components, leading to a loss of MMP (depolarisation) [76]. The antioxidant system mitigates ROS. SOD-2 converts mitochondrial superoxide into hydrogen peroxide, which is further detoxified by Catalase and glutathione peroxidase into water and oxygen [18,35]. Although we found that ROS production of chondrocytes is significantly increased in ME group than C group (Fig. 1**c** and **d**), the protein level of SOD-2 was not significantly decreased in ME group when compared with C group (Fig. 6**a** and **b**). This suggests that there is no marked decrease in MMP of chondrocytes in ME group due to the protein level of SOD-2 is not changed between two groups. On the other hand, the higher protein level of SOD-2 in chondrocytes is found in the AM group than in the C group (Fig. 6**a** and **b**). This suggests that the MMP of AM group is significantly higher than that of the C group due to the higher protein level of SOD-2 in the AM group.

It is known that PGC-1α induces SIRT-3 expression through ERRα. Meanwhile, SIRT-3 stimulates PGC-1α gene expression via increased CREB phosphorylation, forming a positive feedback loop [77]. Moreover, TFAM is a direct deacetylation substrate of SIRT-3, and SIRT-3 promotes mitochondrial biogenesis by deacetylating TFAM to enhance its expression [78]. Therefore, it is hypothesised that reduced PGC-1α levels in the ME group, compared to the C group (Fig. 6**h** and **i**), may lead to decreased expression of SIRT-3 and TFAM in chondrocytes. However, no significant difference in SIRT-3 and TFAM protein expression was observed between the ME and C groups (Fig 6 **f** and **g**, **j** and **k**). It is recognised that SIRT-3 expression is not solely regulated by PGC-1α [79]. Other transcription factors, such as Nrf2, NF-κB, and SP1, also contribute to its regulation [79]. SP1 can bind to the SIRT-3 promoter to enhance its expression, while NF-κB has been shown to upregulate SIRT-3 by binding to its promoter [79]. Given the lack of difference in SIRT-3 and TFAM expression between the ME and C groups, further investigation is required to elucidate the underlying molecular mechanisms.

The limitation of this study is that we only demonstrated the potential of ADSC-MT in enhancing chondrocyte function for chondrocyte-based articular cartilage tissue engineering *in vitro*. Whether chondrocytes treated with ADSC-MT can be used for articular cartilage defect repair requires further investigation. Future research should evaluate the applicability of ADSC-MT with chondrocytes in 3D scaffolds or hydrogels. We aim to develop biomaterial platforms specifically designed to facilitate and enhance mitochondrial transfer in chondrocytes. These engineered systems will enable investigations into whether ADSC-MT-enhancing biomaterials combined with chondrocytes can support therapeutic applications in chondrocyte-based articular cartilage tissue engineering, particularly by improving regenerative outcomes in cartilage defect repair.

Conclusions

In this study, we found that ADSC-MT improves the chondrogenic phenotype by ameliorating mitochondrial dysfunction in senescent chondrocytes. These findings provide a novel strategy to improve the chondrocyte phenotype in senescent chondrocytes prior to their utilisation in chondrocyte-based articular cartilage tissue engineering.

List of abbreviations

ADSCs, adipose-derived stem cells; MT, mitochondrial transfer; ADSC-MT, adipose-derived stem cell mitochondrial transfer; SA-β-gal, senescence-associated β-galactosidase; Col-II, collagen type II; Col-I, collagen type I; 8-OHdG, 8-hydroxydeoxyguanosine; MMP, mitochondrial membrane potential; OA, osteoarthritis; ROS, reactive oxygen species; MSCs, mesenchymal stem cells; MQC, mitochondrial quality control; NEAA, nonessential amino acids; ITS, insulin–transferrin–selenium; PBS, phosphate-buffered saline; C, control; ME, monolayer-expanded; AM, ADSC-MT; DAPI, 4′,6-diamidino-2-phenylindole; OCR, oxygen consumption rate; ECAR, extracellular acidification rate; FCCP, carbonyl cyanide 4-trifluoromethoxy-phenylhydrazone; 2-DG, 2-deoxyglucose; PER, proton efflux rate; real-time PCR, real-time polymerase chain reaction; GAPDH, glyceraldehyde-3-phosphate-dehydrogenase; SOD-2, superoxide dismutase-2; PGC-1α, peroxisome proliferator–activated receptor γ coactivator 1α; SIRT-3, sirtuin-3; SIRT-1, sirtuin-1; COX IV, cytochrome c oxidase IV; VDAC-1, voltage-dependent anion channel 1; PINK-1, PTEN-induced kinase 1; MFN-1, mitofusin 1; MFN-2, mitofusin 2; OPA-1, optic atrophy 1; HRP, horseradish peroxidase; ELISA, enzyme-linked immunosorbent assay; IHC, immunohistochemistry; SEM, standard error of the mean; ANOVA, one-way analysis of variance; TFAM, transcription factor A; ACI, autologous chondrocyte implantation; CDK, cyclin-dependent kinase; mtDNA, mitochondrial DNA; LKB1, liver kinase B1.

Availability of Data and Materials

The data of this study are available from the corresponding author.

Author Contributions

CWW and SCW contributed to the design of this work. CWW, YHH, PLS, LHC, CCL, CHC, YCF, MLH, JKC, and SCW contributed to the interpretation of data.

CWW, YHH, PLS, LHC, CCL, CHC, YCF, MLH, JKC, and SCW analyzed the data. CWW, YHH, and SCW drafted the work. CWW and SCW revised critically for important intellectual content. All authors read and approved the final manuscript. All authors agree to be accountable for all aspects of the work in ensuring that questions related to the accuracy or integrity of any part of the work are appropriately investigated and resolved.

Ethics Approval and Consent to Participate

Human adipose tissue was obtained from patients with prior approval from the Institutional Review Board (IRB) of Kaohsiung Medical University Chung-Ho Memorial Hospital. (Approval Number: KMUHIRB-E(II)-20220292).

Acknowledgments

The authors would like to thank the Center for Research Resources and Development (CRRD) of Kaohsiung Medical University for their assistance in our confocal image analysis. The graphic abstract was generated with the assistance of Microsoft Copilot, which contributed to the illustration process. No scientific data has been generated or modified using AI.

Funding

The authors acknowledge the grant support for this study provided by the National Science Council (MOST 109-2314-B-037-144, NSC 110-2314-B-037-031, NSC 110-2314-B-037-034-MY3 and NSC 113-2314-B-037-083).

Conflict of Interest

The authors declare no conflict of interest.

References

[1] Zhang H, Zhou Z, Zhang F, Wan C. Hydrogel-Based 3D Bioprinting Technology for Articular Cartilage Regenerative Engineering. Gels (Basel, Switzerland). 2024; 10: 430. https://doi.org/10.3390/gels10070430.

[2] Komarraju A, Goldberg-Stein S, Pederson R, McCrum C, Chhabra A. Spectrum of common and uncommon causes of knee joint hyaline cartilage degeneration and their key imaging features. European journal of radiology. 2020; 129: 109097. https://doi.org/10.1016/j.ejrad.2020.109097.

[3] Kloppenburg M, Berenbaum F. Osteoarthritis year in review 2019: epidemiology and therapy. Osteoarthritis and cartilage. 2020; 28: 242–248. https://doi.org/10.1016/j.joca.2020.01.002.

[4] Davies RL, Kuiper NJ. Regenerative Medicine: A Review of the Evolution of Autologous Chondrocyte Implantation (ACI) Therapy. Bioengineering (Basel, Switzerland). 2019; 6: 22. https://doi.org/10.3390/bioengineering6010022.

[5] Jia Z, Wang J, Li X, Yang Q, Han J. Repair Effect of siRNA Double Silencing of the Novel Mechanically Sensitive Ion Channels Piezo1 and TRPV4 on an Osteoarthritis Rat Model. Current molecular pharmacology. 2024; 17: e18761429317745. https://doi.org/10.2174/0118761429317745241017114020.

[6] Hollander JM, Goraltchouk A, Liu J, Xu E, Luppino F, McAlindon TE, *et al*. Single Injection AAV2-FGF18 Gene Therapy Reduces Cartilage Loss and Subchondral Bone Damage in a Mechanically Induced Model of Osteoarthritis. Current gene therapy. 2024; 24: 331–345. https://doi.org/10.2174/0115665232275532231213063634.

[7] Zhang M, Campbell T, Falcon S, Wang J. Regulatory role of NFAT1 signaling in articular chondrocyte activities and osteoarthritis pathogenesis. Biocell. 2023; 47: 2125–2132. https://doi.org/10.32604/biocell.2023.030161.

[8] Makris EA, Gomoll AH, Malizos KN, Hu JC, Athanasiou KA. Repair and tissue engineering techniques for articular cartilage. Nature reviews. Rheumatology. 2015; 11: 21–34. https://doi.org/10.1038/nrrheum.2014.157.

[9] Hulme CH, Perry J, McCarthy HS, Wright KT, Snow M, Mennan C, *et al*. Cell therapy for cartilage repair. Emerging topics in life sciences. 2021; 5: 575–589. https://doi.org/10.1042/ETLS20210015.

[10] Schulze-Tanzil G. Activation and dedifferentiation of chondrocytes: implications in cartilage injury and repair. Annals of anatomy = Anatomischer Anzeiger: official organ of the Anatomische Gesellschaft. 2009; 191: 325–338. https://doi.org/10.1016/j.aanat.2009.05.003.

[11] Fares MY, Daher M, Boufadel P, Haikal E, Haj Shehade T, Koa J, *et al*. The use of autologous chondrocyte transplantation for the treatment of osteoarthritis: a systematic review of clinical trials. Cell and Tissue Bank. 2024; 26: 5. https://doi.org/10.1007/s10561-024-10154-z.

[12] Welsh BL, Sikder P. Advancements in Cartilage Tissue Engineering: A Focused Review. Journal of biomedical materials research. Part B, Applied biomaterials. 2025; 113: e35520. https://doi.org/10.1002/jbm.b.35520.

[13] Ashraf S, Cha BH, Kim JS, Ahn J, Han I, Park H, *et al*. Regulation of senescence associated signaling mechanisms in chondrocytes for cartilage tissue regeneration. Osteoarthritis Cartilage. 2016; 24: 196–205. https://doi.org/10.1016/j.joca.2015.07.008.

[14] Charlier E, Deroyer C, Ciregia F, Malaise O, Neuville S, Plener Z, *et al*. Chondrocyte dedifferentiation and osteoarthritis (OA). Biochem Pharmacol. 2019; 165: 49–65. https://doi.org/10.1016/j.bcp.2019.02.036.

[15] Caron MM, Emans PJ, Coolsen MM, Voss L, Surtel DA, Cremers A, *et al*. Redifferentiation of dedifferentiated human articular chondrocytes: comparison of 2D and 3D cultures. Osteoarthritis and Cartilage. 2012; 20: 1170–1178. https://doi.org/10.1016/j.joca.2012.06.016.

[16] Roberts S, Menage J, Sandell LJ, Evans EH, Richardson JB. Immunohistochemical study of collagen types I and II and procollagen IIA in human cartilage repair tissue following autologous chondrocyte implantation. The Knee. 2009; 16: 398–404. https://doi.org/10.1016/j.knee.2009.02.004.

[17] Di Micco R, Krizhanovsky V, Baker D, d'Adda di Fagagna F. Cellular senescence in ageing: from mechanisms to therapeutic opportunities. Nature reviews. Molecular cell biology. 2021; 22: 75–95. https://doi.org/10.1038/s41580-020-00314-w.

[18] Picca A, Mankowski RT, Burman JL, Donisi L, Kim JS, Marzetti E, *et al*. Mitochondrial quality control mechanisms as molecular targets in cardiac ageing. Nature reviews. Cardiology. 2018; 15: 543–554. https://doi.org/10.1038/s41569-018-0059-z.

[19] Bai Y, Gong X, Dou C, Cao Z, Dong S. Redox control of chondrocyte differentiation and chondrogenesis. Free radical biology & medicine. 2019; 132: 83–89. https://doi.org/10.1016/j.freeradbiomed.2018.10.443

[20] Balaban RS, Nemoto S, Finkel T. Mitochondria, oxidants, and aging. Cell. 2005; 120: 483–495. https://doi.org/10.1016/j.cell.2005.02.001.

[21] Heywood HK, Lee DA. Monolayer expansion induces an oxidative metabolism and ROS in chondrocytes. Biochemical and biophysical research communications. 2008; 373: 224–229. https://doi.org/10.1016/j.bbrc.2008.06.011.

[22] Heywood HK, Lee DA. Low oxygen reduces the modulation to an

oxidative phenotype in monolayer-expanded chondrocytes. Journal of cellular physiology. 2010; 222: 248–253. https://doi.org/10.1002/jcp.21946.

[23] Iorio R, Petricca S, Mattei V, Delle Monache S. Horizontal mitochondrial transfer as a novel bioenergetic tool for mesenchymal stromal/stem cells: molecular mechanisms and therapeutic potential in a variety of diseases. Journal of translational medicine. 2024; 22: 491. https://doi.org/10.1186/s12967-024-05047-4.

[24] Torralba D, Baixauli F, Sánchez-Madrid F. Mitochondria Know No Boundaries: Mechanisms and Functions of Intercellular Mitochondrial Transfer. Frontiers in cell and developmental biology. 2016; 4: 107. https://doi.org/10.3389/fcell.2016.00107.

[25] Hsu YC, Wu YT, Yu TH, Wei YH. Mitochondria in mesenchymal stem cell biology and cell therapy: From cellular differentiation to mitochondrial transfer. Semin Cell Dev Biol. 2016; 52: 119–131. https://doi.org/10.1016/j.semcdb.2016.02.011.

[26] Acquistapace A, Bru T, Lesault PF, Figeac F, Coudert AE, le Coz O, *et al*. Human mesenchymal stem cells reprogram adult cardiomyocytes toward a progenitor-like state through partial cell fusion and mitochondria transfer. Stem Cells. 2011; 29: 812–824. https://doi.org/10.1002/stem.632.

[27] Masuzawa A, Black KM, Pacak CA, Ericsson M, Barnett RJ, Drumm C, *et al*. Transplantation of autologously derived mitochondria protects the heart from ischemia-reperfusion injury. American journal of physiology. Heart and circulatory physiology. 2013; 304: H966–982. https://doi.org/10.1152/ajpheart.00883.2012.

[28] Morrison TJ, Jackson MV, Cunningham EK, Kissenpfennig A, McAuley DF, O'Kane CM, *et al*. Mesenchymal Stromal Cells Modulate Macrophages in Clinically Relevant Lung Injury Models by Extracellular Vesicle Mitochondrial Transfer. American journal of respiratory and critical care medicine. 2017; 196: 1275–1286. https://doi.org/10.1164/rccm.201701-0170OC.

[29] Meng HY, Lu V, Khan W. Adipose Tissue-Derived Mesenchymal Stem Cells as a Potential Restorative Treatment for Cartilage Defects: A PRISMA Review and Meta-Analysis. Pharmaceuticals (Basel, Switzerland). 2021; 14: 1280. https://doi.org/10.3390/ph14121280.

[30] Murata D, Fujimoto R, Nakayama K. Osteochondral Regeneration Using Adipose Tissue-Derived Mesenchymal Stem Cells. International journal of molecular sciences. 2020; 21: 3589. https://doi.org/10.3390/ijms21103589.

[31] Mori D, Miyagawa S, Kawamura T, Yoshioka D, Hata H, Ueno T, *et al*. Mitochondrial Transfer Induced by Adipose-Derived Mesenchymal Stem Cell Transplantation Improves Cardiac Function in Rat Models of Ischemic Cardiomyopathy. Cell Transplant. 2023; 32: 9636897221148457. https://doi.org/10.1177/09636897221148457.

[32] Liu D, Gao Y, Liu J, Huang Y, Yin J, Feng Y, *et al*. Intercellular mitochondrial transfer as a means of tissue revitalization. Signal Transduction and Targeted Therapy. 2021; 6: 65. https://doi.org/10.1038/s41392-020-00440-z.

[33] Wang ZB, Hao JX, Meng TG, Guo L, Dong MZ, Fan LH, *et al*. Transfer of autologous mitochondria from adipose tissue-derived stem cells rescues oocyte quality and infertility in aged mice. Aging (Albany NY). 2017; 9: 2480–2488. https://doi.org/10.18632/aging.101332.

[34] Noh S-E, Lee SJ, Lee TG, Park K-S, Kim JH. Inhibition of cellular senescence hallmarks by mitochondrial transplantation in senescence-induced ARPE-19 cells. Neurobiology of Aging. 2023; 121: 157–165. https://doi.org/https://doi.org/10.1016/j.neurobiolaging.2022.11.003.

[35] Cheung C, Tu S, Feng Y, Wan C, Ai H, Chen Z. Mitochondrial quality control dysfunction in osteoarthritis: Mechanisms, therapeutic strategies & future prospects. Archives of gerontology and geriatrics. 2024; 125: 105522. https://doi.org/10.1016/j.archger.2024.105522.

[36] Chang JK, Chang LH, Hung SH, Wu SC, Lee HY, Lin YS, *et al*. Parathyroid hormone 1-34 inhibits terminal differentiation of human articular chondrocytes and osteoarthritis progression in rats. Arthritis and rheumatism. 2009; 60: 3049–3060. https://doi.org/10.1002/art.24843.

[37] Chen HT, Lee MJ, Chen CH, Chuang SC, Chang LF, Ho ML, *et al*. Proliferation and differentiation potential of human adipose-derived mesenchymal stem cells isolated from elderly patients with osteoporotic fractures. Journal of cellular and molecular medicine. 2012; 16: 582–593. https://doi.org/10.1111/j.1582-4934.2011.01335.x.

[38] Wu SC, Chen CH, Wang JY, Lin YS, Chang JK, Ho ML. Hyaluronan size alters chondrogenesis of adipose-derived stem cells via the CD44/ERK/SOX-9 pathway. Acta Biomaterialia. 2018; 66: 224–237. https://doi.org/10.1016/j.actbio.2017.11.025.

[39] Ho ML, Hsu CJ, Wu CW, Chang LH, Chen JW, Chen CH, *et al*. Enhancement of Osteoblast Function through Extracellular Vesicles Derived from Adipose-Derived Stem Cells. Biomedicines. 2022; 10: 1752. https://doi.org/10.3390/biomedicines10071752.

[40] Wu SC, Huang PY, Chen CH, Teong B, Chen JW, Wu CW, *et al*. Hyaluronan microenvironment enhances cartilage regeneration of human adipose-derived stem cells in a chondral defect model. International journal of biological macromolecules. 2018; 119: 726–740. https://doi.org/10.1016/j.ijbiomac.2018.07.054.

[41] Lin YT, Chen ST, Chang JC, Teoh RJ, Liu CS, Wang GJ. Green extraction of healthy and additive free mitochondria with a conventional centrifuge. Lab on a Chip. 2019; 19: 3862–3869. https://doi.org/10.1039/c9lc00633h.

[42] Guo Y, Chi X, Wang Y, Heng BC, Wei Y, Zhang X, *et al*. Mitochondria transfer enhances proliferation, migration, and osteogenic differentiation of bone marrow mesenchymal stem cell and promotes bone defect healing. Stem cell research & therapy. 2020; 11: 245. https://doi.org/10.1186/s13287-020-01704-9.

[43] Wu SC, Hsiao HF, Ho ML, Hung YL, Chang JK, Wang GJ, *et al*. Suppression of discoidin domain receptor 1 expression enhances the chondrogenesis of adipose-derived stem cells. American journal of physiology. Cell physiology. 2015; 308: C685–C696. https://doi.org/10.1152/ajpcell.00398.2014.

[44] Wu SC, Chen CH, Chang JK, Fu YC, Wang CK, Eswaramoorthy R, *et al*. Hyaluronan initiates chondrogenesis mainly via CD44 in human adipose-derived stem cells. J Appl Physiol (1985). 2013; 114: 1610–1618. https://doi.org/japplphysiol.01132.2012.

[45] Wu SC, Chang JK, Wang CK, Wang GJ, Ho ML. Enhancement of chondrogenesis of human adipose derived stem cells in a hyaluronan-enriched microenvironment. Biomaterials. 2010; 31: 631–640. https://doi.org/10.1016/j.biomaterials.2009.09.089.

[46] Wang CZ, Chen SM, Chen CH, Wang CK, Wang GJ, Chang JK, *et al*. The effect of the local delivery of alendronate on human adipose-derived stem cell-based bone regeneration. Biomaterials. 2010; 31: 8674–8683. https://doi.org/10.1016/j.biomaterials.2010.07.096.

[47] Chang LH, Wu SC, Chen CH, Wang GJ, Chang JK, Ho ML. Parathyroid hormone 1-34 reduces dexamethasone-induced terminal differentiation in human articular chondrocytes. Toxicology. 2016; 368–369: 116–128. https://doi.org/10.1016/j.tox.2016.09.002.

[48] Livak KJ, Schmittgen TD. Analysis of relative gene expression data using real-time quantitative PCR and the 2(-Delta Delta C(T)) Method. Methods. 2001; 25: 402–408. https://doi.org/10.1006/meth.2001.1262.

[49] Guo C, Li X, Wang R, Yu J, Ye M, Mao L, *et al*. Association between Oxidative DNA Damage and Risk of Colorectal Cancer: Sensitive Determination of Urinary 8-Hydroxy-2'-deoxyguanosine by UPLC-MS/MS Analysis. Scientific reports. 2016; 6: 32581. https://doi.org/10.1038/srep32581.

[50] Kadenbach B, Hüttemann M, Arnold S, Lee I, Bender E. Mitochondrial energy metabolism is regulated via nuclear-coded subunits of cytochrome c oxidase. Free radical biology & medicine. 2000; 29: 211–221. https://doi.org/10.1016/s0891-5849(00)00305-1.

[51] Camara AKS, Zhou Y, Wen PC, Tajkhorshid E, Kwok WM. Mitochondrial VDAC1: A Key Gatekeeper as Potential Therapeutic Tar-

get. Frontiers in physiology. 2017; 8: 460. https://doi.org/10.3389/fphys.2017.00460.
[52] Rim YA, Nam Y, Ju JH. The Role of Chondrocyte Hypertrophy and Senescence in Osteoarthritis Initiation and Progression. International journal of molecular sciences. 2020; 21: 2358. https://doi.org/10.3390/ijms21072358.
[53] Yue L, Lim R, Owens BD. Latest Advances in Chondrocyte-Based Cartilage Repair. Biomedicines. 2024; 12: 1367. https://doi.org/10.3390/biomedicines12061367.
[54] Roseti L, Cavallo C, Desando G, D'Alessandro M, Grigolo B. Forty Years of the Use of Cells for Cartilage Regeneration: The Research Side. Pharmaceutics. 2024; 16: 1622. https://doi.org/10.3390/pharmaceutics16121622.
[55] Tang Q, Zheng G, Feng Z, Chen Y, Lou Y, Wang C, *et al*. Trehalose ameliorates oxidative stress-mediated mitochondrial dysfunction and ER stress via selective autophagy stimulation and autophagic flux restoration in osteoarthritis development. Cell death & disease. 2017; 8: e3081. https://doi.org/10.1038/cddis.2017.453.
[56] Miwa S, Kashyap S, Chini E, von Zglinicki T. Mitochondrial dysfunction in cell senescence and aging. The Journal of clinical investigation. 2022; 132: e158447. https://doi.org/10.1172/JCI158447.
[57] Bhatti JS, Bhatti GK, Reddy PH. Mitochondrial dysfunction and oxidative stress in metabolic disorders — A step towards mitochondria based therapeutic strategies. Biochimica et biophysica acta. Molecular basis of disease. 2017; 1863: 1066–1077. https://doi.org/https://doi.org/10.1016/j.bbadis.2016.11.010.
[58] Cloonan SM, Kim K, Esteves P, Trian T, Barnes PJ. Mitochondrial dysfunction in lung ageing and disease. European respiratory review: an official journal of the European Respiratory Society. 2020; 29: 200165. https://doi.org/10.1183/16000617.0165-2020.
[59] Clemente-Suárez VJ, Martin-Rodriguez A, Yanez-Sepulveda R, Tornero-Aguilera JF. Mitochondrial Transfer as a Novel Therapeutic Approach in Disease Diagnosis and Treatment. International journal of molecular sciences. 2023; 24: 8848. https://doi.org/10.3390/ijms24108848.
[60] Liu Q, Zhang X, Zhu T, Xu Z, Dong Y, Chen B. Mitochondrial transfer from mesenchymal stem cells: Mechanisms and functions. Mitochondrion. 2024; 79: 101950. https://doi.org/10.1016/j.mito.2024.101950.
[61] Shanmughapriya S, Langford D, Natarajaseenivasan K. Inter and Intracellular mitochondrial trafficking in health and disease. Ageing research reviews. 2020; 62: 101128. https://doi.org/10.1016/j.arr.2020.101128.
[62] Konari N, Nagaishi K, Kikuchi S, Fujimiya M. Mitochondria transfer from mesenchymal stem cells structurally and functionally repairs renal proximal tubular epithelial cells in diabetic nephropathy in vivo. Scientific reports. 2019; 9: 5184. https://doi.org/10.1038/s41598-019-40163-y.
[63] Clark MA, Shay JW. Mitochondrial transformation of mammalian cells. Nature. 1982; 295: 605–607. https://doi.org/10.1038/295605a0.
[64] Scott JL, Gabrielides C, Davidson RK, Swingler TE, Clark IM, Wallis GA, *et al*. Superoxide dismutase downregulation in osteoarthritis progression and end-stage disease. Annals of the rheumatic diseases. 2010; 69: 1502–1510. https://doi.org/10.1136/ard.2009.119966.
[65] Gavriilidis C, Miwa S, von Zglinicki T, Taylor RW, Young DA. Mitochondrial dysfunction in osteoarthritis is associated with downregulation of superoxide dismutase 2. Arthritis and Rheumatism. 2013; 65: 378–387. https://doi.org/10.1002/art.37782.
[66] Son JM, Sarsour EH, Kakkerla Balaraju A, Fussell J, Kalen AL, Wagner BA, *et al*. Mitofusin 1 and optic atrophy 1 shift metabolism to mitochondrial respiration during aging. Aging Cell. 2017; 16: 1136–1145. https://doi.org/10.1111/acel.12649.
[67] Chen H, Chomyn A, Chan DC. Disruption of fusion results in mitochondrial heterogeneity and dysfunction. The Journal of biological chemistry. 2005; 280: 26185–26192. https://doi.org/10.1074/jbc.M503062200.
[68] Chen H, Vermulst M, Wang YE, Chomyn A, Prolla TA, McCaffery JM, *et al*. Mitochondrial fusion is required for mtDNA stability in skeletal muscle and tolerance of mtDNA mutations. Cell. 2010; 141: 280–289. https://doi.org/10.1016/j.cell.2010.02.026.
[69] Griparic L, van der Wel NN, Orozco IJ, Peters PJ, van der Bliek AM. Loss of the intermembrane space protein Mgm1/OPA1 induces swelling and localized constrictions along the lengths of mitochondria. The Journal of biological chemistry. 2004; 279: 18792–18798. https://doi.org/10.1074/jbc.M400920200.
[70] Zanna C, Ghelli A, Porcelli AM, Karbowski M, Youle RJ, Schimpf S, *et al*. OPA1 mutations associated with dominant optic atrophy impair oxidative phosphorylation and mitochondrial fusion. Brain: a journal of neurology. 2008; 131: 352–367. https://doi.org/10.1093/brain/awm335.
[71] Civiletto G, Varanita T, Cerutti R, Gorletta T, Barbaro S, Marchet S, *et al*. Opa1 overexpression ameliorates the phenotype of two mitochondrial disease mouse models. Cell Metabolism. 2015; 21: 845–854. https://doi.org/10.1016/j.cmet.2015.04.016.
[72] Li J, Lai M, Zhang X, Li Z, Yang D, Zhao M, *et al*. PINK1-parkin-mediated neuronal mitophagy deficiency in prion disease. Cell death & disease. 2022; 13: 162. https://doi.org/10.1038/s41419-022-04613-2.
[73] Sarraf SA, Raman M, Guarani-Pereira V, Sowa ME, Huttlin EL, Gygi SP, *et al*. Landscape of the PARKIN-dependent ubiquitylome in response to mitochondrial depolarization. Nature. 2013; 496: 372–376. https://doi.org/10.1038/nature12043.
[74] Ansari MY, Khan NM, Ahmad I, Haqqi TM. Parkin clearance of dysfunctional mitochondria regulates ROS levels and increases survival of human chondrocytes. Osteoarthritis and Cartilage. 2018; 26: 1087–1097. https://doi.org/10.1016/j.joca.2017.07.020.
[75] Wang Z, Xu T, Sun Y, Zhang X, Wang X. AMPK/PGC-1alpha and p53 modulate VDAC1 expression mediated by reduced ATP level and metabolic oxidative stress in neuronal cells. Acta biochimica et biophysica Sinica. 2024; 56: 162–173. https://doi.org/10.3724/abbs.2024012.
[76] Jing W, Liu C, Su C, Liu L, Chen P, Li X, *et al*. Role of reactive oxygen species and mitochondrial damage in rheumatoid arthritis and targeted drugs. Frontiers in immunology. 2023; 14: 1107670. https://doi.org/10.3389/fimmu.2023.1107670.
[77] Kong X, Wang R, Xue Y, Liu X, Zhang H, Chen Y, *et al*. Sirtuin 3, a new target of PGC-1alpha, plays an important role in the suppression of ROS and mitochondrial biogenesis. PLoS One. 2010; 5: e11707. https://doi.org/10.1371/journal.pone.0011707.
[78] Liu H, Li S, Liu X, Chen Y, Deng H. SIRT3 Overexpression Inhibits Growth of Kidney Tumor Cells and Enhances Mitochondrial Biogenesis. Journal of proteome research. 2018; 17: 3143–3152. https://doi.org/10.1021/acs.jproteome.8b00260.
[79] Peng X, Ni H, Kuang B, Wang Z, Hou S, Gu S, *et al*. Sirtuin 3 in renal diseases and aging: From mechanisms to potential therapies. Pharmacological research. 2024; 206: 107261. https://doi.org/10.1016/j.phrs.2024.107261.

Editor's note: The Scientific Editor responsible for this paper was Martin Stoddart.

Received: 26th February 2025; **Accepted**: 17th March 2026; **Published**: 29th May 2026